AIRCRAFT ACCIDENT REPORT 7/2010

Air Accidents Investigation Branch

Department for Transport

Report on the accident to Aerospatiale (Eurocopter) AS 332L Super Puma registration G-PUMI at Aberdeen Airport, Scotland on 13 October 2006

This investigation was carried out in accordance with
The Civil Aviation (Investigation of Air Accidents and Incidents) Regulations 1996

The sole objective of the investigation of an accident or incident under these Regulations shall be the prevention of accidents and incidents. It shall not be the purpose of such an investigation to apportion blame or liability.

Published with the permission of the Department for Transport (Air Accidents Investigation Branch).

This report contains facts which have been determined up to the time of publication. This information is published to inform the aviation industry and the public of the general circumstances of accidents and serious incidents.

Published 23 November 2010

Printed in the United Kingdom for the Air Accidents Investigation Branch

Department for Transport
Air Accidents Investigation Branch
Farnborough House
Berkshire Copse Road
Aldershot
Hampshire GU11 2HH

October 2010

The Right Honourable Philip Hammond
Secretary of State for Transport

Dear Secretary of State

I have the honour to submit the report by Mr R D G Carter, an Inspector of Air Accidents, on the circumstances of the accident to Aerospatiale (Eurocopter) AS 332L Super Puma, registration G-PUMI at Aberdeen Airport on 13 October 2006.

Yours sincerely

Keith Conradi
Chief Inspector of Air Accidents

Contents

Appendices

GLOSSARY OF ABBREVIATIONS USED IN THIS REPORT

AAIB	Air Accidents Investigation Branch
ABT	Advanced Blade tracker
AD	Airworthiness Directive
AFS	Aerodrome Fire Service
ATC	Air Traffic Control
ATIS	Automatic Terminal Information System
BEA	Bureau d'Enquêtes et d'Analyses
CAA	Civil Aviation Authority
CAM	Cockpit Area Microphone
CAVOK	Ceiling And Visibility OK (for VFR flight)
°C,F,M,T	Degrees Celsius, Fahrenheit, magnetic, true
CVFDR	Cockpit Voice Flight Data Recorder
EASA	European Aviation Safety Agency
EDX	energy dispersive analysis
FE	finite element
FEA	finite element analysis
FEM	finite element model
FOD	foreign object damage
g	acceleration due to Earth's gravity
hr(s)	hour(s) (clock time as in 1200 hrs)
HUMS	Health and Usage Monitoring System
ICAO	International Civil Aviation Organization
IHUMS	Integrated Health and Usage Monitoring System
kt	knot(s)
LPC	Licence Proficiency Check
MDR	Maintenance Data Recorder
MHz	megahertz
mm	millimetre(s)
MPa	megapascal
MTOM	Maximum Take Off Mass
N	Newtons
N_R	Main rotor rotation speed (rotorcraft)
nm	nautical mile(s)
OPC	Operator Proficiency Check
SEM	scanning electron microscope
UTC	Co-ordinated Universal Time (GMT)
UTS	ultimate stensile strength
µm	micrometre
V_{max}	maximum airspeed
V_{NE}	never exceed airspeed

Air Accidents Investigation Branch

Aircraft Accident Report No: 7/2010 (EW/C2006/10/06)

Registered Owner and Operator: Bristow Helicopters Limited

Aircraft Type and model: Aerospatiale (Eurocopter) AS 332L Super Puma

Nationality: United Kingdom

Registration: G-PUMI

Place of Incident: Aberdeen Airport, Scotland

Date and Time: 13 October 2006 at 1220 hrs

Synopsis

The accident was notified to the Air Accidents Investigation Branch (AAIB) by the Operator's Flight Safety Officer. The following Inspectors participated in the investigation:

Mr R D G Carter	Investigator-in-charge
Mr C A Protheroe	Engineering
Miss G M Dean	Operations
Mr P Wivell	Flight Recorders

The aircraft was departing from Runway 14 for a flight to oil platforms in the North Sea, carrying 13 passengers. Five seconds into the takeoff the crew heard a bang and an abnormal vibration started. The crew rejected the takeoff and landed back on the runway. The aircraft started to taxi but the severe vibration continued so the commander stopped and shut down the helicopter on the threshold of Runway 32.

Initial examination showed that one main rotor blade spindle had fractured, through the lower section of its attachment yoke on the leading side of the spindle. Post-fracture plastic deformation of the lug had stretched open the fracture, separating the faces by some 12 mm.

As a result of this accident the helicopter manufacturer published an Emergency Alert Service Bulletin, requiring periodic inspections, and this was subsequently mandated by the European Aviation Safety Agency (EASA) as an Airworthiness Directive. In July 2009

the manufacturer issued Service Bulletins which introduced a 'wet' assembly procedure, with new nuts, for the main rotor blade spindles. This eliminated the requirement for the repetitive inspection procedure and was made mandatory by the issue of an Airworthiness Directive (AD) by the EASA.

The investigation identified the following causal factors for the failure of the spindle yoke:

(i) Wear on the flapping hinge inner race.

(ii) Excessive clamping pre-load across the yoke, due to the tie bolt being torqued to the specified dry value in the presence of grease when it was reinstalled some 175 hours prior to failure of the yoke.

(iii) Significant hoop stresses in the bore of the yoke due to adverse tolerance stacking and the associated interference fit of the bush in the yoke.

The following were considered as contributory factors in the failure:

(i) Flight loads biased towards the high-speed level flight condition, slightly higher than those generated by normal level flight cruise conditions.

(ii) A minor deviation in corner radius profile at the inner end of the bore of the yoke, with a small increase in the attendant stress concentration.

(iii) A minor reduction, at the fatigue origin site, in the intensity of the compressive surface layer stresses from the shot-peen process.

(iv) Flight loads in the spindle yoke slightly higher than anticipated in certification fatigue testing, due to the action of the lead-lag dampers (frequency adaptors).

One Safety Recommendation is made, to the EASA, concerning HUMS detection in helicopter rotating systems.

1. Factual Information

1.1 History of the flight

The helicopter had completed two flights earlier in the day with a different operating crew and neither crew member had observed anything unusual during the flights.

This flight was planned to depart from Aberdeen at 1200 hrs; the first destination was the Britannia Platform (N5802.9 E00108.3) 118 nm north-east of Aberdeen and then the flight was to continue to a second platform nearby, before returning to Aberdeen. The commander, once he had been advised of the payload, loaded fuel to take the weight up to the Maximum Take Off Mass (MTOM), thus ensuring there would be enough fuel to complete the round trip flight. The weather forecast was good with CAVOK conditions at both platforms.

The helicopter was started and at 1158 hrs the crew, using call sign Bristow 62A, called for clearance to taxi to the passenger boarding area. Passenger boarding was carried out with the rotors running, in accordance with normal operating procedures, and was completed at 1212 hrs. The co-pilot then advised ATC that they were ready for taxi and the helicopter was given clearance to taxi to holding point C2. Five minutes later the helicopter was cleared to taxi to C3 and the crew were advised to expect departure from Runway 16. After a further five minutes ATC asked whether they could accept departure from Runway 14 and the crew confirmed that they could.

The helicopter was cleared to line up on Runway 14. When lined up the commander handed control to the co-pilot, who was to be the handling pilot for the first sector. When clearance was received the co-pilot lifted into the hover, the power was cross-checked by the commander and the takeoff began.

The crew were using a calculated 'stop/go' time of seven seconds (Tcrit); five seconds into the takeoff they heard a bang and an abnormal vibration started. The commander made an exclamation, took over control and rejected the takeoff. He made a radio call to advise ATC that they were rejecting and included the information that it was because of vibration and a loud bang; ATC acknowledged. The helicopter landed back on Runway 14, close to the intersection with Runway 16. After a few moments the commander called ATC for instructions and was advised to continue ahead and cross Runway 16. The helicopter continued towards the end of Runway 14 but because the vibration continued to be severe the commander decided he must shut down and advised ATC accordingly. The helicopter was shut down on the threshold of Runway 32.

During the incident the controller continued to manage other traffic movements, which included giving clearances to land for a helicopter on Runway 23 and another aircraft on Runway 16.

As soon as ATC realised the helicopter would be shutting down, a ground incident was declared. The Airport Fire Service (AFS) was alerted and deployed onto the airfield. One aircraft on final approach for Runway 16, which had already received landing clearance, was instructed to go around to allow a fire vehicle to cross the threshold.

After the rotors had stopped the passengers were disembarked into a waiting bus. The helicopter was towed into a maintenance hangar for further investigation.

1.2 Injuries to persons

Injuries	Crew	Passengers	Others
Fatal	-	-	-
Serious	-	-	-
None	2	13	-

1.3 Damage to the aircraft

The 'Blue' main rotor blade spindle had fractured through the lower section of its attachment yoke on the leading side of the spindle, and post-fracture plastic deformation of the lug had stretched open the fracture, separating the faces by some 12 mm (Figure 1). A sacrificial washer bonded to the inner face of the lug was also fractured on a plane broadly parallel with that of the lug fracture, but displaced from it slightly inboard. Dark deposits, visually consistent with fretting or corrosion debris, were present on and around the fractures.

Some 90% of the lug failure exhibited clearly defined 'beach mark' striations and surface-staining consistent with fatigue crack propagation in service, from an origin at, or close to, the corner radius at the junction of the bore in the yoke (that holds the hinge pin which allows blade 'flapping' articulation) and the inner face of the yoke. The remaining 10% of the fracture comprised a shear lip, evidently formed as this surviving portion of the cracked section fractured in overload.

1.4 Other damage

None.

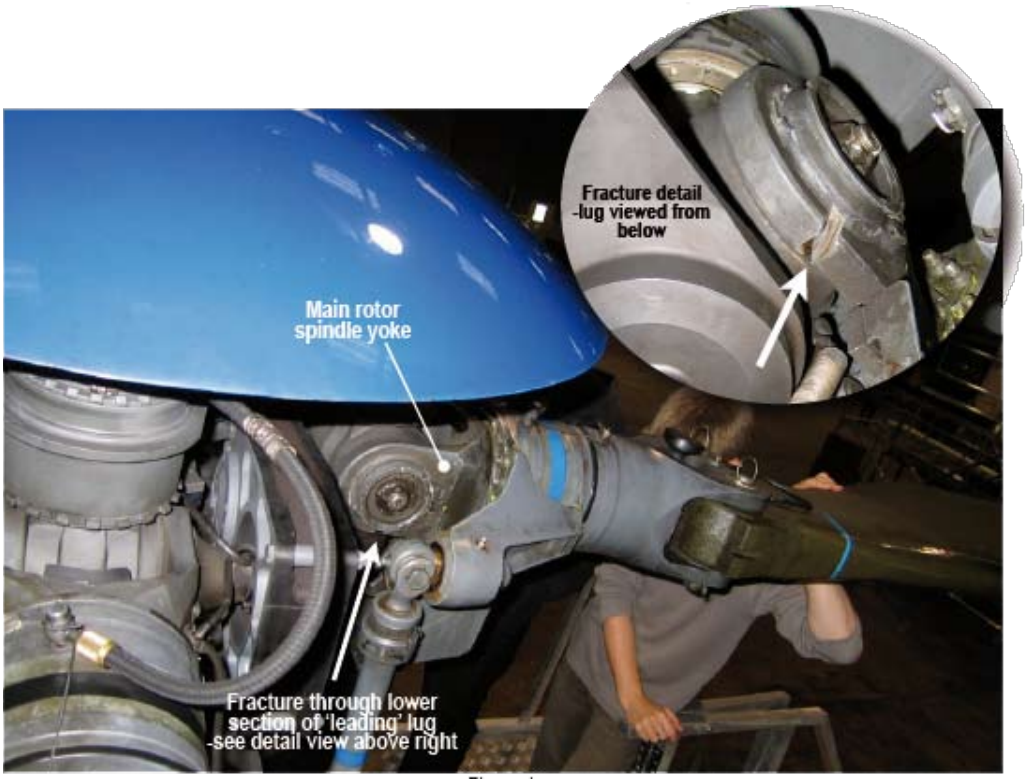

Figure 1

Location of yoke fracture

1.5 Personnel information

1.5.1 Commander

Male aged 40 years

Licence:	Airline Transport Pilot's Licence (H)
OPC/ LPC renewed:	4/5 October 2006
Annual line check:	9 November 2005
Medical certificate:	Class 1 valid
Flying experience:	7,800 hours (of which 7,550 hours were on type)
	Last 90 days - 210 hours
	Last 28 days - 59 hours
Time reported for duty:	0700 hours
Previous rest period:	16 hours 15 minutes

1.5.2 Co-pilot

Male aged 23 years

Licence:	Commercial Pilot's Licence (H)
OPC renewed:	18 June 2006
Medical certificate:	Class 1 valid
Flying experience:	455 hours (of which 92 hours were on type) Last 90 days - 67 hours Last 28 days - 67 hours
Time reported for duty:	0545 hours
Previous rest period:	13 hours

The co-pilot was undergoing line training with the operator.

1.6 Aircraft information

1.6.1 General information

Aircraft type	Aerospatiale (Eurocopter) AS 332L Super Puma
Engines	2 x Turbomeca Makila 1A turboshaft engines
Manufacture	Built 1985, Serial N° 2170
Registration	G-PUMI, registered to Bristow Helicopters Ltd
Cert of Airworthiness	EASA Standard Certificate of Airworthiness
Airframe hours	22,687 hrs since manufacture; 1,558 hrs since last major (C Check, completed 15 July 2005); 171 hrs since last main rotor head '750 hr' inspection

1.6.2 Rotor system

1.6.2.1 Rotor head configuration

The main rotor system in the AS 332L has a fully-articulated head, carrying four composite blades attached to root fittings by removable pins. Blade pitch is controlled by a conventional swashplate, connected by pushrods to control horns bolted to each blade-root fitting. Figure 2a shows the general arrangement of the head (blades omitted for clarity).

'Lead-lag' (drag) damping of each blade is provided by elastomeric dampers, known as frequency adaptors, connected to the trailing end of the flapping hinge spindles, and anchored to lugs on the rotor mast. At the time of the accident, G-PUMI was equipped with the latest variant of flapping hinge and frequency damper, illustrated in Figure 2b.

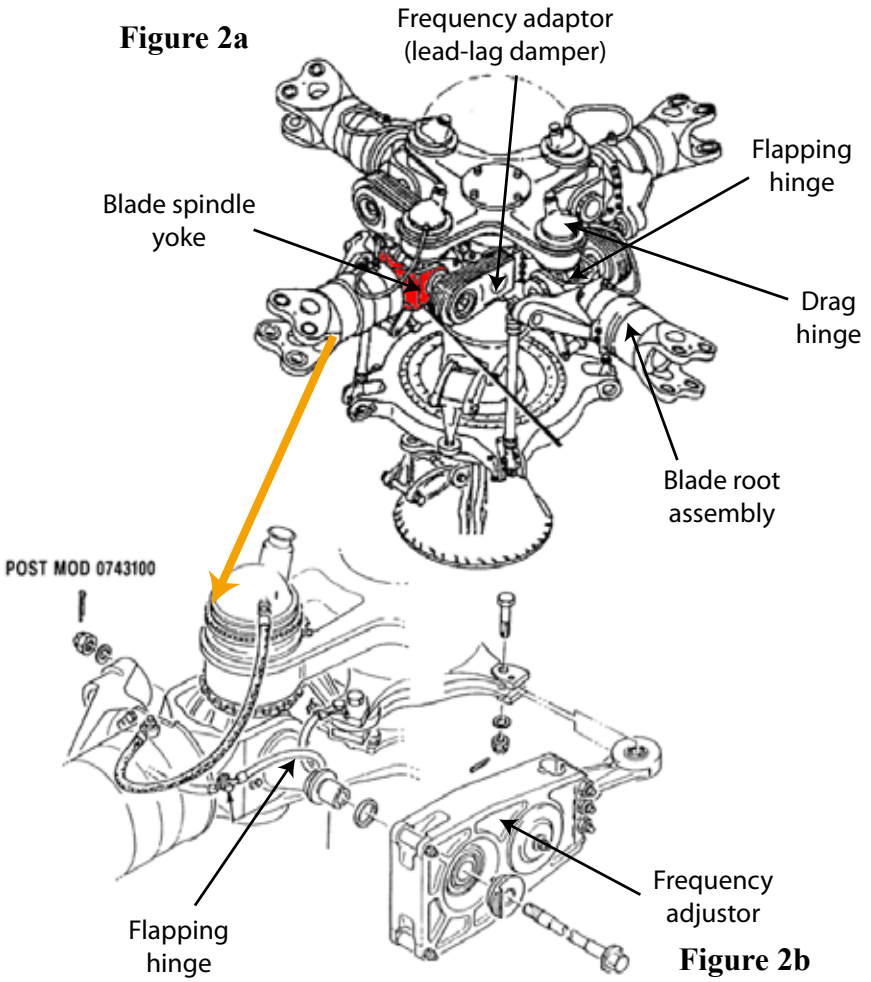

Figures 2a and 2b

Figure 2a - Generic Super Puma rotor head
Figure 2b - Type of flapping hinge & frequency adaptor installed on G-PUMI

The blade attachment fittings comprise an outer 'feathering' sleeve, to which the blades are attached by removable pins, and an inner spindle, incorporating an integrally-formed yoke, connecting it to the hub portion of the rotor head. The sleeve section, carrying the blade, is connected to the spindle by a combination of thrust and pitch change bearings. These provide restraint against the centrifugal forces acting on the blade, whilst allowing changes of blade pitch to take place, controlled through conventional pitch horns bolted to the sleeve.

The blade attachment spindle forms the outer half of a 'hook joint' that facilitates both the flapping and lead-lag articulation of the blade as a whole; the spindle yoke provides the flapping articulation and a corresponding yoke fitting built into

the rotor hub provides the lead-lag articulation. The 'spider' fitting connecting the two comprises a (vertical) lead-lag hinge pin with a thickened central portion that accommodates a separate (horizontal) 'flapping' hinge pin.

1.6.2.2 Blade spindles

The blade spindle is machined from a steel forging (Figure 3). The bore in the lug portions of the yoke is protected at the interface with the flapping hinge pin by steel bushings. The inner and outer faces of the lugs are protected by large steel washers, coated on their wear surfaces with a layer of sintered tungsten carbide, designed to protect the fitting proper against fretting damage.

The blade spindle had undergone a series of evolutionary design changes since its inception on the original SA 330 variant of the Puma. Details of these changes are provided later in this report in Appendix A, one being the increase of lug thickness from 15 mm to 20 mm.

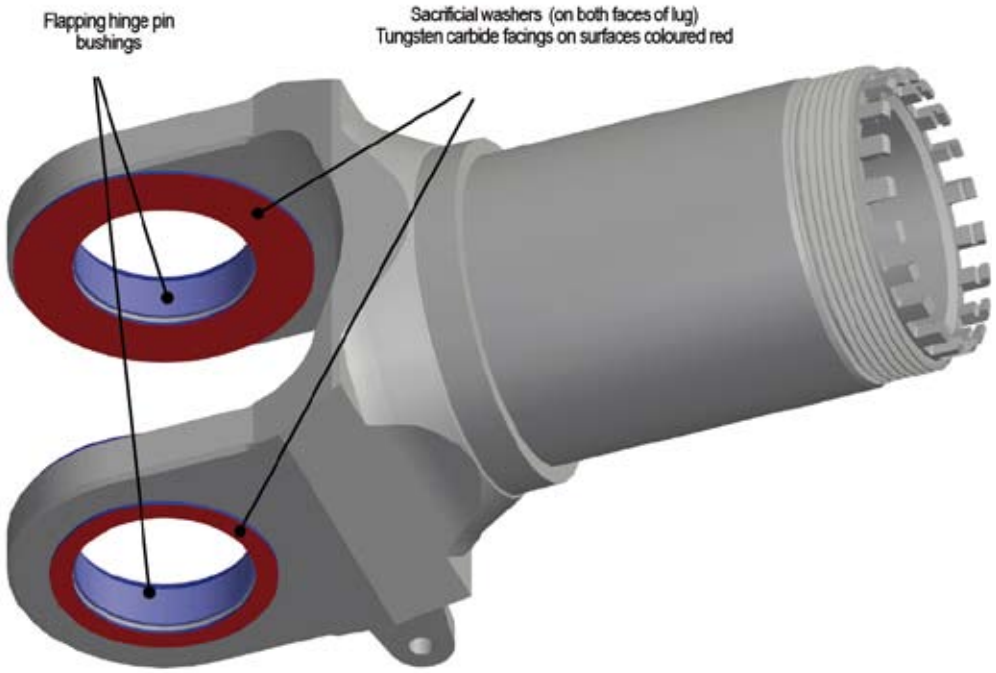

Figure 3

Form of the blade spindle, and location of sacrificial washers and bushings

1.6.3 Maintenance and service history

1.6.3.1 Main rotor head assembly service history

The main rotor head assembly[1] was installed in G-PUMI on 4 July 2005, during a C check. No abnormal adjustments of the rotor system were required during or immediately after installation, and the aircraft's documentation subsequently recorded no unusual or significant maintenance activity affecting the main rotor system.

No significant in-service events were recorded during the interval between installation of the overhauled head assembly and the spindle failure on 13 October 2006. Specifically, there was no record of bird-strike, foreign object damage (FOD) or lightning strike, no sudden rotor stoppages or rotor speed exceedences were reported and none were apparent in the IHUMS record. All recorded maintenance activity affecting the head was routine and is summarised in Table 1 (overleaf).

1.6.4 Main blade spindle life limits

The variant of blade spindle installed on G-PUMI was lifed at 8,000 hours, with an overhaul interval of 1,500 hours.

At the time of the accident, the spindle was operating on a permitted extension of 10% of the overhaul deadline (to 1,650 hrs), and had accumulated a total of 1,556 hours since its last overhaul. It had undergone one overhaul, and had accumulated a total time since manufacture of 3,032 hrs. The aircraft was scheduled for planned maintenance activity on the day after the accident, which included removal of the spindle in question for overhaul.

1.7 Meteorological information

The meteorological conditions at the Britannia platform at 1141 hrs were observed as CAVOK with a southerly surface wind.

Aberdeen Airport ATIS information 'Uniform' issued at 1150 hrs was: Runway 16 in use, surface wind from 200° at 13 kt, varying between 170° and 230°, CAVOK, temperature 15°C, dewpoint 11°C and pressure 1029 mb. The surface wind immediately prior to takeoff was from 190° at 11 kt.

1 Part N° 332A31-0001-05, serial N° M188, zero time since overhaul).

Date	Hrs prior to spindle failure	Action
30 Jun 2005 to 15 Jul 2005	1558	**C check:** Main rotor head assembly replaced with overhauled unit Routine post-installation set-up, and post-'C check' acceptance test flight adjustments
20 Jul 2005	1539	**IHUMS adjustments:** Track rods, black up 7, blue up 2 red up 5 clicks. Mass, black +150 and blue +150 grammes. Tabs, blue up 5 and red up 6 degrees.
26 Sep 2005	1275	Red pitch change horn eye bolt bearings worn beyond limits; horn replaced.
28 Sep 2005	1266	Red pitch change horn replaced (OPS requirement).
6 Dec 2005	1064	Red MRB taken to service another aircraft; replaced with serviceable blade. Yellow MRB replaced.
16 Dec 2005	1067	**IHUMS adjustments carried out:** Black pitch rod -9; blue pitch rod -6; red pitch rod -7. '+250 added to g to black'; yellow tab up 5 deg; red tab up 4 deg.
28 Jan 2006	932	**Main rotor head 750 hr inspection**. All 8 main rotor blade attachment pins worn beyond limits, and replaced.
10 Sep 2006	203	**Main rotor blades removed for 750 hr inspection**. All eight blade attachment pins found corroded & replaced >>Leading edge S/steel strip cracked; blade replaced
10 Sep 2006	171	**Main rotor head 750 hr inspection**. Red pitch change horn eye bolt replaced (worn to specified limits) All four frequency adaptors replaced (worn to specified limits)
9 Oct 2006	32.5	**IHUMS adjustment carried out:-** Black blade pitch rod adjusted down 2 clicks

Table 1

Summary of routine maintenance activity relating to the rotor head

1.8 Aids to navigation

Not applicable.

1.9 Communications

Communications between the helicopter and ATC were recorded. The first recorded communication for call sign Bristow 62A was when taxi clearance was requested from Ground Movement Control on frequency 121.7 MHz and the helicopter was transferred to Aberdeen Tower frequency 118.1 MHz at 1218 hours. The helicopter was cleared to lift into the hover at the threshold of Runway 14 and then to take off at 1225 hrs.

Following the incident, ATC requested that the helicopter contact the AFS on frequency 121.60 MHz but no transmissions were made on this frequency.

1.10 Aerodrome information

There are a large number of helicopters based at Aberdeen Airport, principally for the purpose of supplying services to offshore oil and gas platforms.

Where the helicopter stopped on the threshold of Runway 32 was within the protected area of Runway 16 and after the incident the helicopter was towed away to a safe area. The Airport re-opened for traffic after about 10 minutes and there were no diversions.

1.11 Flight recorders

The helicopter carried a Cockpit Voice Flight Data Recorder (CVFDR)[2] which recorded five hours of data and one hour of three-channel audio: commander, co-pilot and Cockpit Area Microphone (CAM). The data and audio were successfully downloaded from the recorder and covered the entire accident flight. The audio quality was such that many 'pops' were recorded from the start of the recording until they disappeared during the taxi to the terminal before picking up the passengers and the CAM appeared to be recording at a reduced volume from that of a previous flight. The operator later corrected problems found with the aircraft systems associated with the audio recording.

The aircraft was fitted with an Integrated Health and Usage Monitoring System (IHUMS). IHUMS gathers CVFDR-type data, along with additional parameters generated by the Advanced Blade Tracker (ABT) and multiple vibration sensors. A Maintenance Data Recorder (MDR) was used to record CVFDR parameters, along with snapshots of ABT and vibration data gathered when specific flight characteristics were met. The MDR data was regularly transferred to a ground station for automatic detection of exceedences and trend analysis.

The ABT involved the use of sensors and processing equipment to measure blade tracking information both in flapping and lead-lag.

1.11.1 CVFDR recordings

The CVFDR recordings for this flight started at a recorded time of 1140 hrs (UTC) and the ATIS information 'Uniform' was recorded at 1150 hours. At 1152 hrs the engine start was initiated and the aircraft then taxied to pick up passengers before taxiing for a Runway 14 departure.

2 Penny & Giles CVFDR, part number 900/D51506.

As the aircraft was cleared for an immediate takeoff from Runway 14, with a wind of 180/13 kt, the commander counted down from "SIX". At 1224:52 hrs, as the commander said "TWO", a thud was recorded on the CVR and heard by the crew. At this point the airspeed was approximately 21 kt and the groundspeed was 11 kt. The longitudinal and lateral accelerations then started oscillating with a peak-to-peak value of approximately 0.2 g and a period of 2.5 seconds. Two to three seconds after the thud, the commander called "REJECTING" and "I HAVE CONTROL" and collective pitch was reduced with an immediate effect on torque and altitude. The airspeed peaked a second or so later, at 49 kt.

The 'weight-on-wheels' condition was triggered 22 seconds after the decision to reject the takeoff. At this point the airspeed had reduced to 20 kt and the ground speed to 21 kt. Just after this, the N_R (main rotor speed) reduced from the steady 99% to a steady 97%. The ground speed reduced further, initially quickly but under 10 kt the deceleration was less marked. At 1226:08 the groundspeed had reduced to zero and the 'normal' (that is, vertical) acceleration became cyclical.

At 1226:20 the commander informed the tower that they would need to shut down as they were "shaking on the spot". Shortly after, the engine power was reduced, with N_R reducing to a steady 75% and the amplitude of the acceleration oscillations also reduced and 15 seconds later, with an N_R of 40%, the rotor brake was applied. 14 seconds after that N_R reached its minimum value and the CVFDR recording stopped at 1231 hrs.

1.11.2 Advanced Blade Tracker (ABT) recordings

No valid ABT data was recorded during the short period the aircraft was in the air, missing the onset of the high vibration period, although data which appeared valid was recorded from a time coinciding with the aircraft settling back on the ground. Assuming that the adjacent (Black and Yellow) blades remained aligned, the limited data in this period appeared to show a small lag of the Blue blade, around 1.5º.

1.11.3 Previous ABT data

The track and lag data from 30 August 2006 to the accident was analysed. This showed a small exceedence of the median track spread on 9 October 2006 and this prompted a small adjustment to the Black blade which was tracking slightly high. This does not appear significant in the context of the accident to G-PUMI and there were no anomalies relating to the Blue blade, which suffered the structural failure on 13 October.

1.11.4 IHUMS limitation

The AAIB held discussions with the supplier of the IHUMS system in G-PUMI and the CAA. These discussions indicated that, without specific sensors attached directly to the component, the onset of a crack, such as that found in G-PUMI, would probably not be detectable as the geometry of the blade would be unlikely to change sufficiently, until complete failure.

1.12 Wreckage information - technical examination

1.12.1 Condition of main rotor head and blades

A detailed visual examination of the main rotor gearbox and rotor head assembly, including the swashplate, control rods and associated hardware, revealed no evidence of any abnormality except for the yoke fracture and localised secondary damage caused by post-fracture deformation of the lug. All four main rotor blades were in good condition and none exhibited signs of damage, or any feature atypical of in-service blades. The flapping hinge pins and their associated tie bolts, and the frequency adaptors, were to the latest modification standard and a visual inspection indicated that all items were in good condition.

1.12.2 Disassembly and preliminary examination of the failed spindle

All four rotor blades were removed and the complete rotor head assembly was then removed from the aircraft to facilitate disassembly and isolation of the fractured blade spindle, part number 332A31 1485.06, serial number FR281. The following observations were made during the disassembly:

1) The measured torque at the flapping hinge tie bolt was 95 lbf-ft: just above the bottom end of the allowable range. Nothing abnormal was found during withdrawal of the flapping hinge pin.

2) Post-fracture deformation of the failed lug had opened the fracture faces by some 12 mm (Figure 4), and enlarged the spanwise diameter of the bore to 71 mm, compared with 66.2 mm measured vertically. The resulting diametral gap, between the flapping spindle and the bore of the lug, is clearly visible at A in Figure 4.

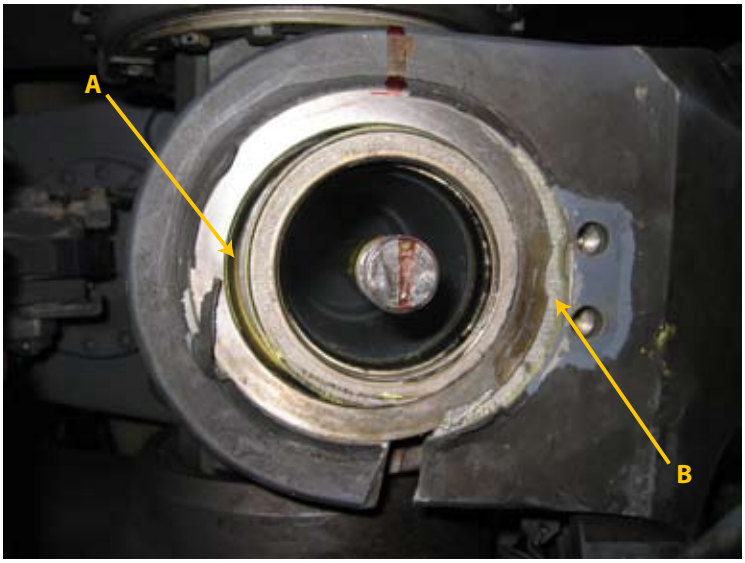

Figure 4

Post-fracture deformation

3) The outboard segment of the outer sacrificial washer on the failed lug had disbonded and moved outboard (region B in Figure 4) as the lug was stretched immediately post-fracture.

4) The sacrificial washer on the inner face of the failed lug was broken into two segments, along a fracture plane parallel with, but displaced slightly outboard from, the plane of the lug fracture (Figure 5).

Figure 5

Wear/corrosion deposits, and position of lug fracture in relation to inner washer fracture

5) Post-fracture deformation of the lug had resulted in the inboard segment of the fractured inner washer rotating in-plane relative to the outer segment, and riding up, and partially over, the outer segment (Figure 6). Figure 6 shows the excised section of the yoke turned back and placed next to the end of the flapping bearing, to expose the two surfaces in contact.

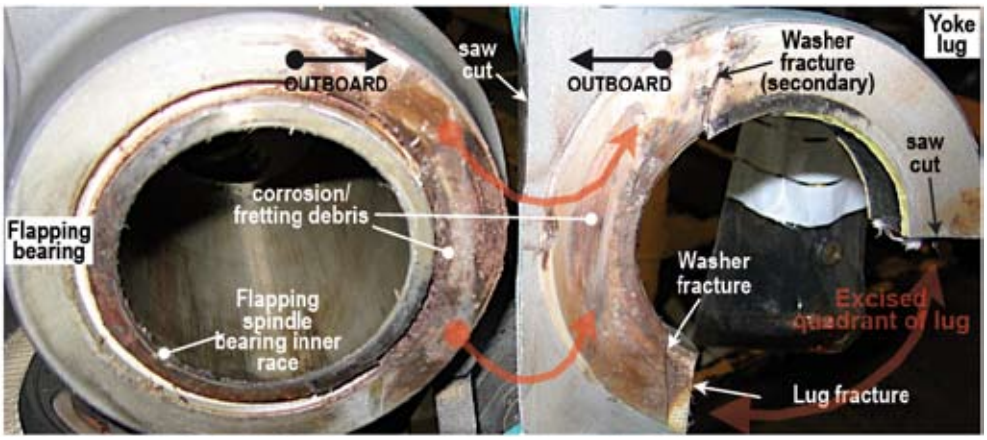

Figure 6

Lug excised from yoke and placed beside mating faces on flapping spindle, showing washer fractures on lug and corresponding patterns of wear and corrosion debris

The inboard segment of the inner washer was disbonded adjacent to both fractures, and wear/corrosion deposits in these areas showed that both the fractures and the adjacent disbonding pre-dated the yoke failure.

6) The yoke fracture faces exhibited very clear growth marks and patterns of staining consistent with progressive fatigue fracture from an origin region at the inner corner of the bore of lug (Figures 7a and 7b). Both fracture faces were generally in good condition, but some slight bruising was discernible in the origin region.

7) Surface corrosion/wear deposits similar to those evident on the fractures on the inner washer on the leading side of the yoke were also present, albeit to a lesser extent, at similar locations on the wear face of the corresponding (intact) washer bonded to the trailing side of the yoke (Figure 8).

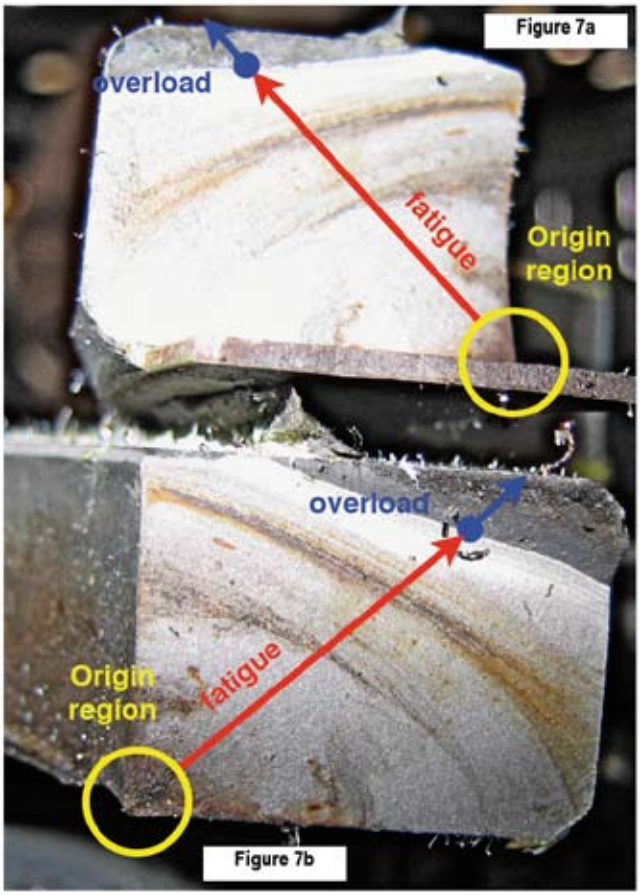

Figure 7a (outboard) and Figure 7b (inboard)

Lug fracture face details

Figure 8

Wear/corrosion deposits on wear face of the intact inner washer on the trailing side of the yoke

8) Regions of corrosion/wear deposits were evident on the outer circumference of the bush from the failed lug, at positions which corresponded with the positions of the fractures in the lug/washer and washer fractures, labelled A and B respectively in Figures 9 and 10.

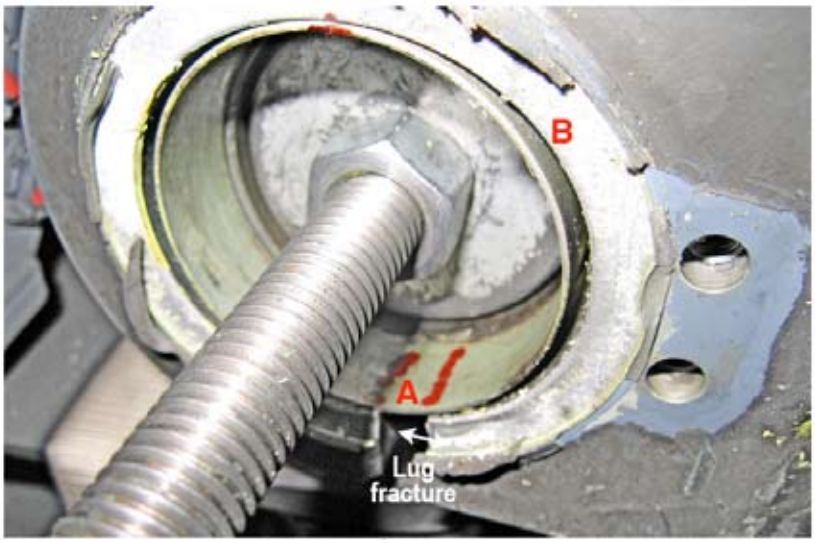

Figure 9

Bush in bore of failed lug, released by post-fracture deformation. A and B show 'o'clock' positions of wear/corrosion deposits on interfacing surface of bush shown in Figures 10a and 10b

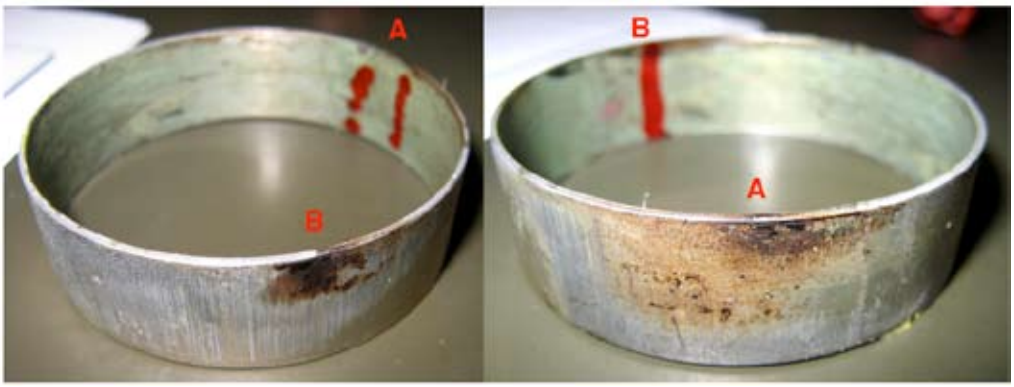

Figures 10a and 10b

Showing locations and extent of wear/corrosion deposits on mating surface of lug bushing (See Figure 9 for positional reference)

1.12.3 Metallurgical examination of the spindle fracture

1.12.3.1 Fracture characteristics

As noted above (Figures 7a and 7b), the fracture surfaces exhibited some slight corrosion and mutual damage, but were generally in good condition. Detailed metallurgical study of the fracture faces, using both optical and scanning electron microscopy (SEM), confirmed that the lug failure was caused by fatigue crack propagation from an origin region at the inner corner of the bore, which penetrated some 90% of the cross-section before the remaining 10% failed in overload.

The fracture surface exhibited a repeated pattern of growth marks (Figure 11a) consistent with a high-cycle mode of propagation overall, interrupted at intervals by short bursts of ductile cracking, each burst consistent with a single load reversal of large magnitude. The banding pattern formed by the interruption (beach) marks at intervals in the high cycle growth was especially clearly defined in the region bounding the final overload rupture (Figure 11b).

Figure 11b

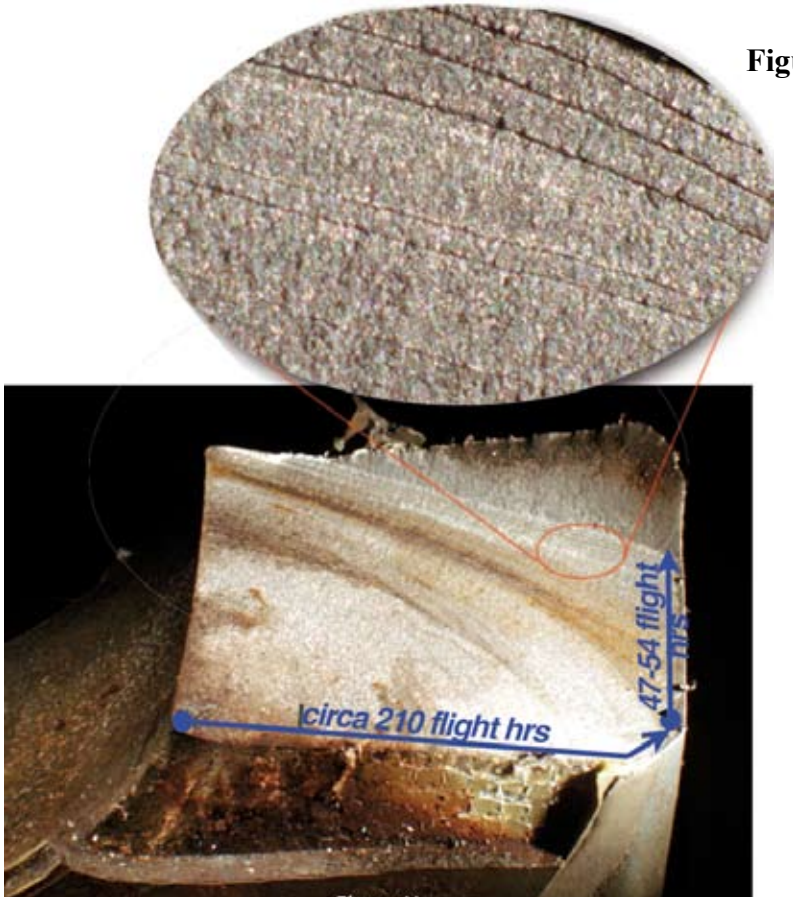

Figure 11a

Banding pattern on fracture face and banding pattern detail

1.12.3.2 Growth rate estimates

The fracture surface banding pattern of fine striations, with beach marks at irregular intervals, was consistent with propagation primarily in response to a substantially regular pattern of in-flight stresses (mostly high-cycle small-amplitude), with variations about a relatively large 'working mean' stress associated with centrifugal loading of the blade. The beach-mark interruptions to this regular pattern of growth would be associated with the large change in mean stress as the rotor centrifugal forces decayed and increased with each rotor stop/start cycle.

Estimates made independently by the AAIB and the manufacturer, based on separate analyses of the two halves of the fracture, suggested that the phase of crack propagation during which the fracture traversed the exposed lower surface of the yoke, and was thus potentially discoverable by visual inspection alone, involved between 15 and 17 flights. According to the aircraft's flight logs, this corresponded to some 47 to 54 flight hours.

The growth bands were much less clearly defined in those regions associated with the preceding stages of propagation, that is, from the point of origin to the stage at which the crack first broke through to the visible lower surface of the yoke; quantitative analysis required extrapolation and an attendant lack of precision. However, it was estimated that this initial phase of growth corresponded to around 73 start cycles, equivalent to some 210 flight hours (based on the flight logs).

The 'best estimate' of the total propagation period, from the origin to final failure, was therefore some 90 rotor starts and 258 flight hours.

1.12.3.3 Potential initiation features

The crack origin

The fracture face close to the origin region exhibited slight, but significant, secondary damage caused by relative movement between the fracture faces as the crack propagated. Consequently it was not possible to establish precisely the crack's origin, or origins.

Under high magnification, the external (as distinct from fracture) surface in the origin region was characterised by a rough and dimpled surface texture overlaid with a number of deeper depressions and pits, particularly around the corner radius at the junction between the face and the bore of the lug (Figure 12).

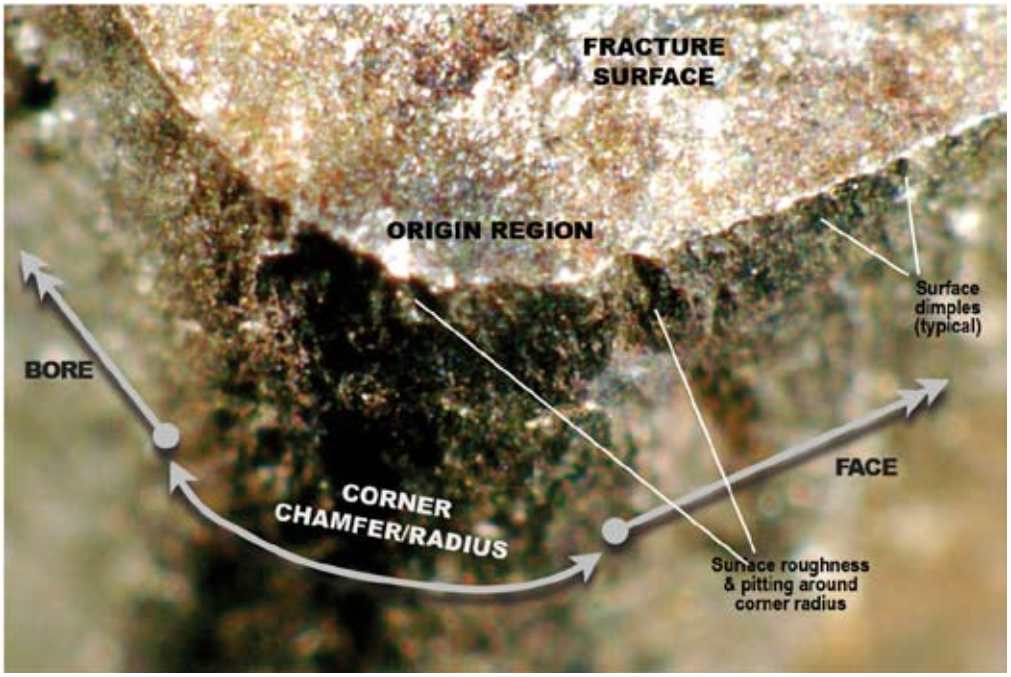

Figure 12

Oblique close-up view of the fatigue crack origin region, showing the surface topography in the bore and on the inner face of the yoke, and at the corner formed between these two surfaces

However, the sizes of these features, and the stress concentrations likely to have been associated with them, were assessed as having been too small to have been solely responsible for initiating the fatigue crack.

Although corrosion was also present in the pitted area, no evidence was found to suggest that the fatigue crack had originated at a corrosion pit.

Sections

One half of the fracture was sectioned on a plane normal to the face, and tangential to the centre, of the corner radius - but set back slightly from it. The section was mounted, and then 'ground back' progressively in stages through the corner region, so as to traverse the crack origin. At each stage of the traverse, the microstructure was examined at high magnification, both in the '*polished'* and the '*polished and etched'* states for any metallurgical or sub-surface feature that had played a causal role in crack initiation. The surface profile was also photographed at each stage.

Surface finish

Figures 13a through 13c show the surface finish of the lug in the general vicinity of the fracture origin and Figure 13d at 180º from the origin.

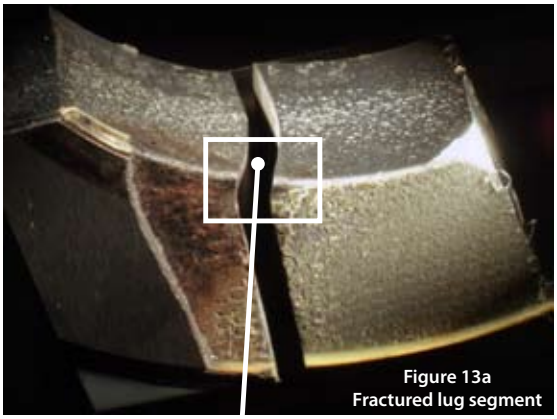

Figure 13a
Fractured lug segment

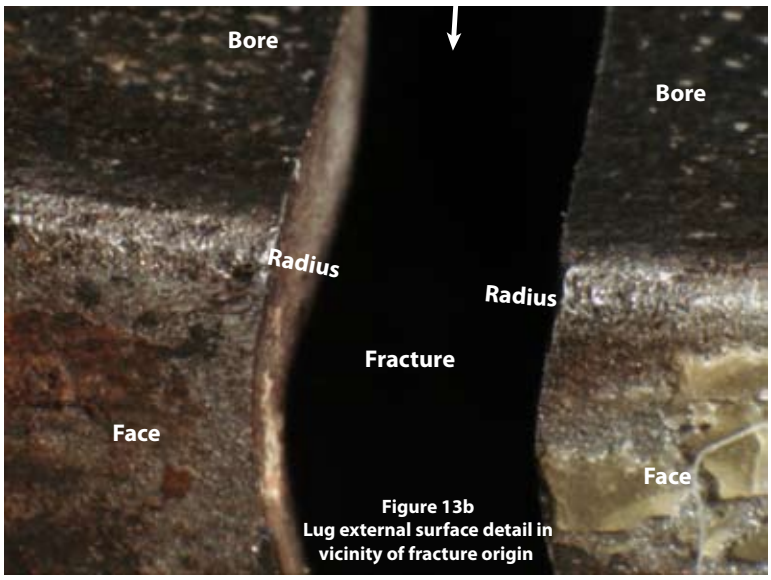

Figure 13b
Lug external surface detail in vicinity of fracture origin

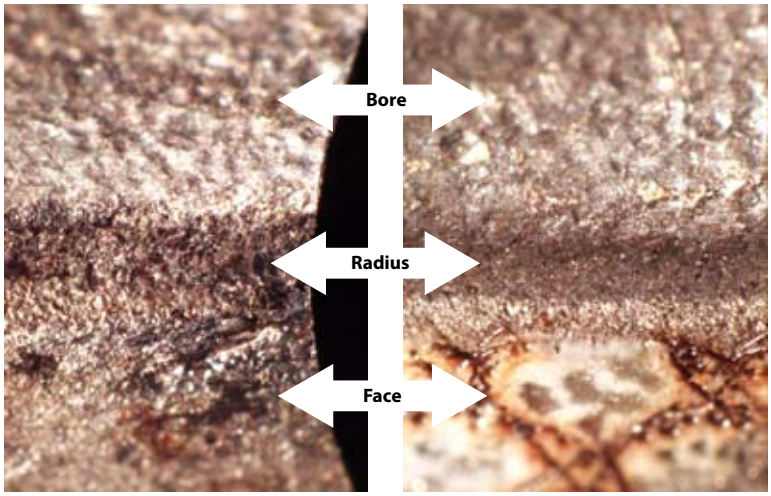

Figure 13c
Radius surface detail at fracture origin

Figure 13d
Radius surface at 180º from fracture origin

Figure 13

At a macroscopic level, the finish in the bore of the lug was rough and irregular, with a dimpled appearance consistent with it have been shot-peened at some stage. Remnants of what appeared to be the adhesive, which bonded the bush to the bore of the lug, were also present,

The face of the lug was partially covered with the remains of the (very tenacious) adhesive mesh-matrix used to fix the sacrificial washer to the face of the yoke, but sufficient of the surface was exposed to see that the face exhibited a finer surface finish than the bore, with less clear evidence of shot-peen dimpling.

The surface of the corner radius in the vicinity of the origin displayed a similar roughness to that of the face. The surface of the corner radius, on the side of the yoke diametrically opposite the fracture origin, was significantly less rough, shown in comparison between Figures 13c and 13d.

Surface profile

The surface finish revealed in the mounted section as it was ground back progressively through the origin region is shown in the sequence of photo-montages at Figure 14.

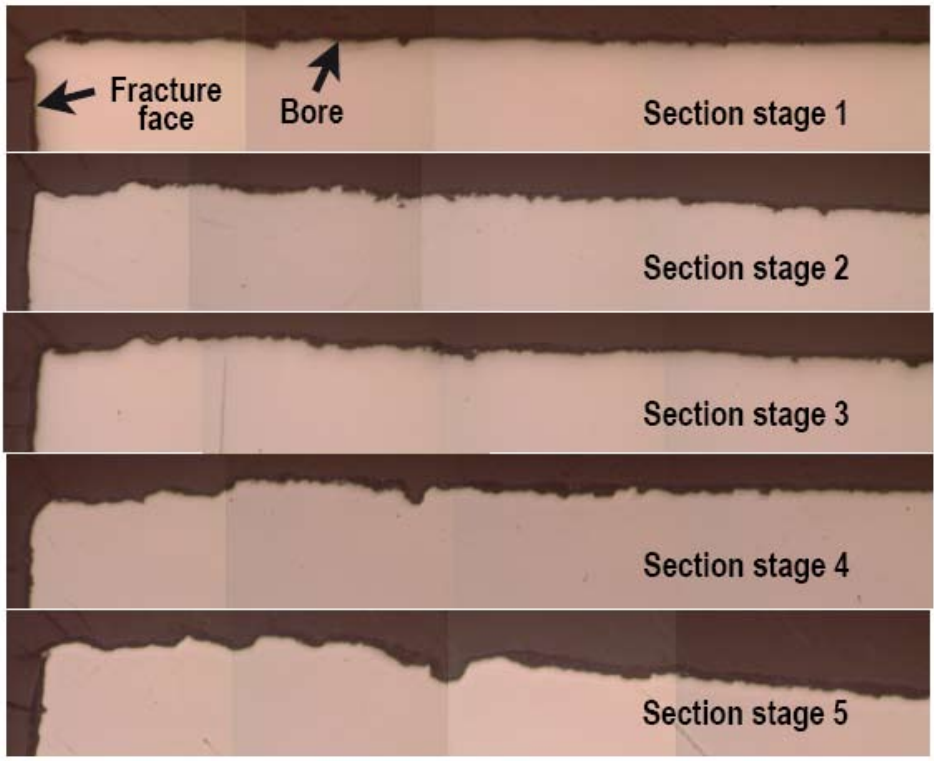

Figure 14

Bore surface profile at successive sections through the origin region

Near the origin, the surface profile was generally sharper and more jagged, consistent with it having been subject to grit-blasting. Further into the bore, away from the corner, the profile was significantly less jagged. Measured relative to the overall surface level, the deepest cavity was approximately 46 µm deep; 35 µm relative to the local surface.

A similar pattern of surface roughness was evident in other polished sections from the failed yoke, taken through an adjoining quadrant of the lug just outboard of the fracture (Figure 15). Evidence was also found in these sections of particles of a silicate material, believed to be blasting grit, entrapped in the surface of the lug in several places.

It is evident from Figure 15 that the corner radius was, in practice, more of a 'chamfer' than a true radius.

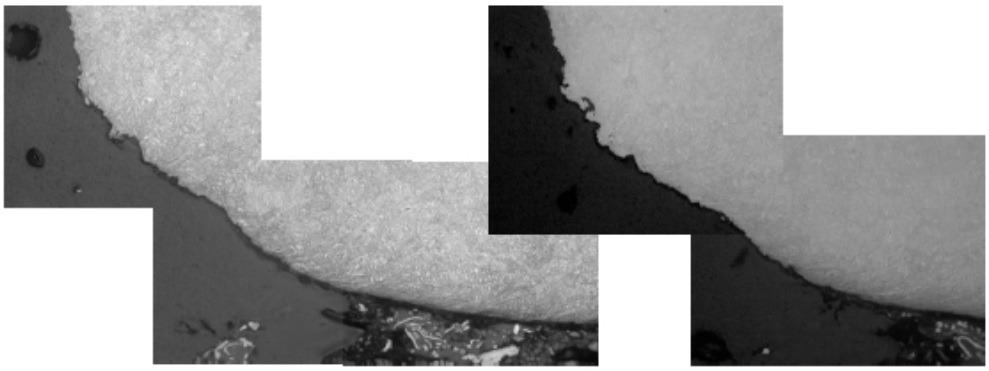

Figure 15

Corner surface profile on section adjacent to fracture plane (bore is to right, and faces towards top, in both photographs)

Micro-structure

The bore interior and the corner radii at the bores were subject to a controlled shot-peen process during manufacture, intended to increase the component's fatigue strength by inducing a residual compressive stress in the sub-surface layer. The mounted and etched sections were therefore examined for evidence of the characteristic grain-deformation pattern that is usually produced by this process, as the surface layer is hammered down by the shot-peen balls.

Evidence of an unusual grain deformation pattern was found in the surface layer of the bore, comprising a compressive deformation of the grain structure combined with a shearing deformation in a direction parallel with the bore

axis, towards the inside corner. The resulting grain-flow gave the appearance of the surface layer having been subject to a combined crushing and smearing of the surface layer into the depth of the bore. This characteristic grain-flow was clearly evident over most of the bore's sub-surface layer, but became less distinct towards the corner radius, and was absent altogether from the corner profile itself. The grain deformation pattern was not typical of that produced by normal shot-peening, with the shot balls impacting normal to the surface. It was, however, suggestive of a shot-peening process in which the axis of bombardment was at some oblique angle to the face of the bore.

From visual observation of the grain-flow, no direct inferences could be drawn as to the magnitude of any associated sub-surface residual stresses, save that the complete absence of any visible deformation in the surface layer around the inner corner region implied a corresponding absence of any compressive residual stress at the fatigue crack origin.

Material properties

The micro-structure was consistent with the material and heat treatement specified by the manufacturer (30NCD16 steel, heat treated at 850°C; annealed at 585°C). Hardness readings on the mounted section indicated a value close to the upper end of the specified range. Destructive testing of the failed lug, to determine the ultimate tensile strength (UTS) was not judged necessary in light of the hardness results, which implied a UTS correspondingly near the upper end of its specified range.

1.12.4 Comparison with exemplar yoke

A blade spindle that was undergoing overhaul at the manufacturer's facility was extracted from the overhaul program and provided to the AAIB to serve as an exemplar for comparison with the failed spindle. This exemplar had already passed through the initial stages of overhaul, which included the separation of all four sacrificial washers and the removal of all surface finishes and adhesives used to bond the bush and sacrificial washers to the yoke, processes which included blast-bead cleaning.

The leading lug of the exemplar yoke was excised and subjected to a similar program of sectioning and examination as the failed item, with particular reference to surface profile, geometry and grain structure at and around the inner corner of the bore, in the region corresponding to the fracture origin.

1.12.4.1 Physical condition

No cracks were present in either lug of the exemplar yoke. It was notable, however, that even after having passed through the preparatory cleaning processes, evidence of residual corrosion/fretting debris was clearly visible on the inner face of the leading lug at positions which corresponded very closely with the positions of the cracks in the sacrificial washer on the failed lug from G-PUMI. Figure 16 shows the lug from the exemplar yoke positioned alongside the failed yoke from G-PUMI, with these features highlighted. The correlation illustrated in Figure 16 strongly suggested that 'as received' for overhaul, the washer on the exemplar lug was cracked at locations similar to that on the lug from G-PUMI. The manufacturer's records did not record the condition of the washer at the time of receipt, but it was understood that a significant proportion of time-expired spindles submitted for overhaul had similarly cracked washers.

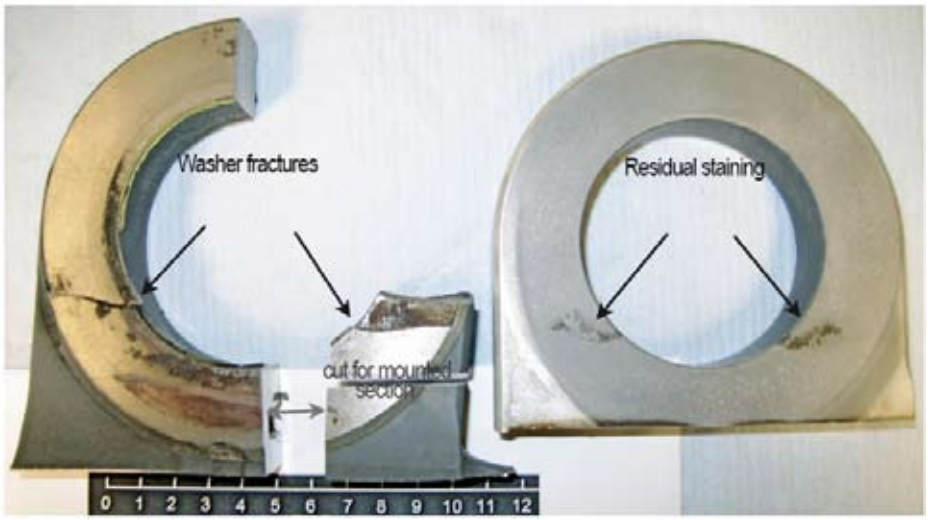

Figure 16

Comparison between position of residual staining on exemplar lug and washer fracture locations on failed lug from G-PUMI spindle.

1.12.4.2 Surface finish and corner profile

There was a clear difference between the surface of the bore and the face of the exemplar lug, see Figure 17a. The bore had a regular dimpled surface texture consistent with that produced by shot-peening, whereas the face displayed a rough, but much finer-textured, finish consistent with it having been grit blasted.

The corner profile itself was more of a chamfer, as called up in the manufacturer's drawings, than the radius profile of the failed lug from G-PUMI.

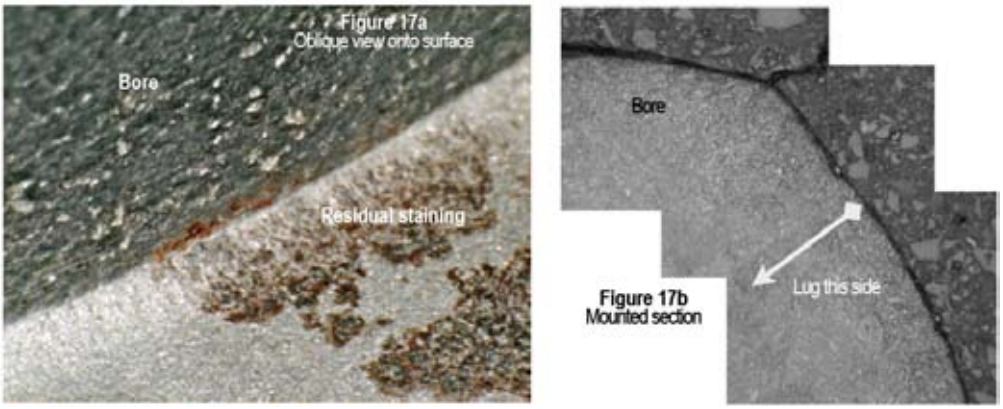

Figures 17a and 17b

Exemplar lug: Surface finish at inner corner of bore at location corresponding to G-PUMI crack origin

1.12.4.3 Material properties

Surface-layer properties

Hardness - A series of micro-hardness traverses was carried out on the transverse metallographic sections from both the failed and the exemplar yokes, using a 100 gram load on a diamond pyramid indenter, along the lines shown in Figure 18. Logarithmic regression curves of the results, obtained from plots of hardness vs distance from the surface of the yoke, showed a consistent difference in the scatter of the hardness values obtained from the exemplar and the failed yokes, shown Figures 19a and 19b, which suggested that the hardness of the failed yoke in the surface region was marginally lower than the exemplar.

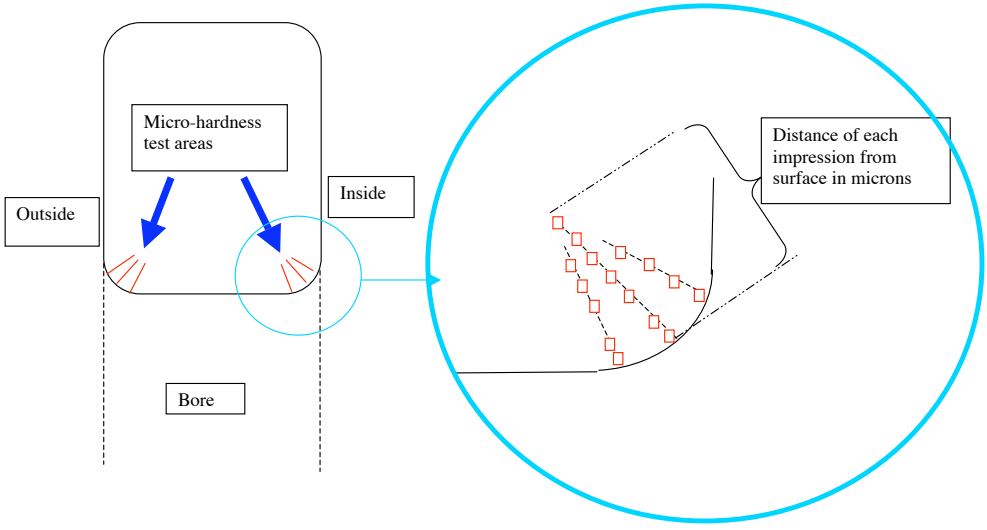

Figure 18

Micro-hardness traverse details

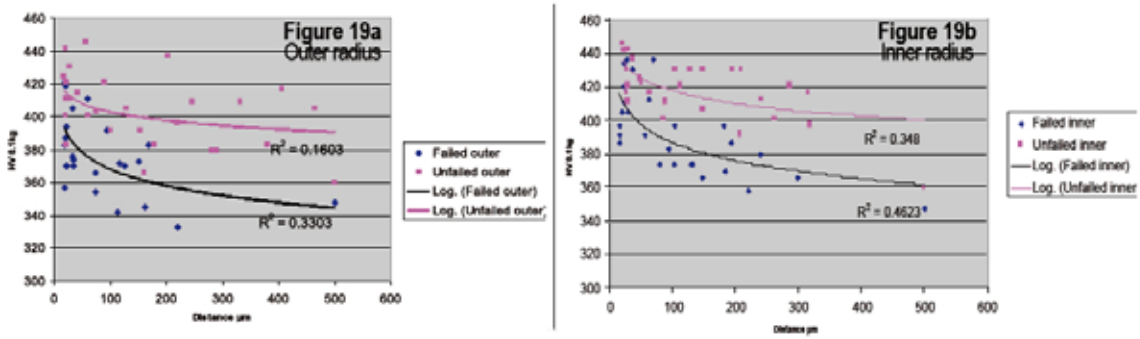

Figures 19a and 19b

Regression curves from plots of hardness vs distance from surface

Residual compressive stress - Measurements of the residual stresses in the surface layer of both the exemplar and the failed lug were made independently by the aircraft manufacturer, and, at the direction of the AAIB, by specialists at the Open University Department of Materials Science. X-ray diffraction techniques were employed in each case, but the equipment and methodologies differed in detail between the two laboratories.

In both cases, the undertaking was problematic in relation to measurements made in close proximity to the corner radius, due to the changing geometry at the intersection between the x-ray beam and the surface of the material as the collimator traversed the edge of the sample.

Measurements taken for the AAIB

Surface and sub-surface residual stresses in the bore

Both the exemplar and the failed lug from G-PUMI exhibited significantly high residual compressive stresses at the surface in the bore of the yoke, see Figure 20.

In the central region of the bore (region A in Figure 20), the failed lug from G-PUMI these stresses measured in the *hoop* direction were of the order of 500 MPa; near the outer face (region C), they were approximately 30% below this value and at the inner corner of the bore, in the region corresponding to the fatigue crack origin (region B), they were some 10% higher.

The exemplar exhibited a similar residual compressive stress distribution in the hoop direction but the stress intensities were generally some 10% higher than those of the failed lug.

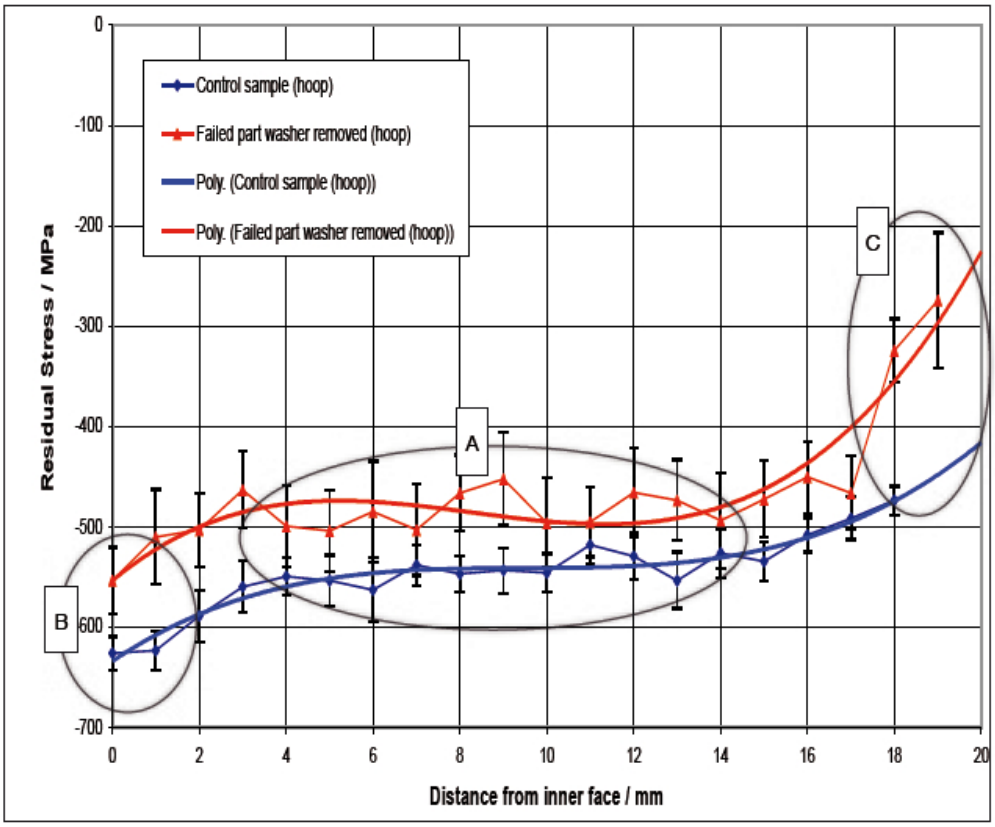

Figure 20

Plot of measured hoop stress in surface of the bore vs distance from inner face of lug

A similar situation was apparent in relation to the residual compressive stress component orientated parallel with the bore axis, at right angles to the hoop component, and also the component at 45° to the bore axis. However, the stresses on these orientations showed a slightly more pronounced difference between the failed and exemplar lugs, the exemplar exhibiting compressive stress intensities some 20% higher than those of the failed lug.

Inner face

The residual compressive stresses measured on the inner face of the failed lug in the hoop, radial, and 45% orientations were slightly lower than the corresponding values measured in the bore, generally at between 350 and 400 MPa. The exemplar showed similar trends, but with magnitudes generally about 20% greater than those in the failed component. Figure 21 shows these trends for the hoop component.

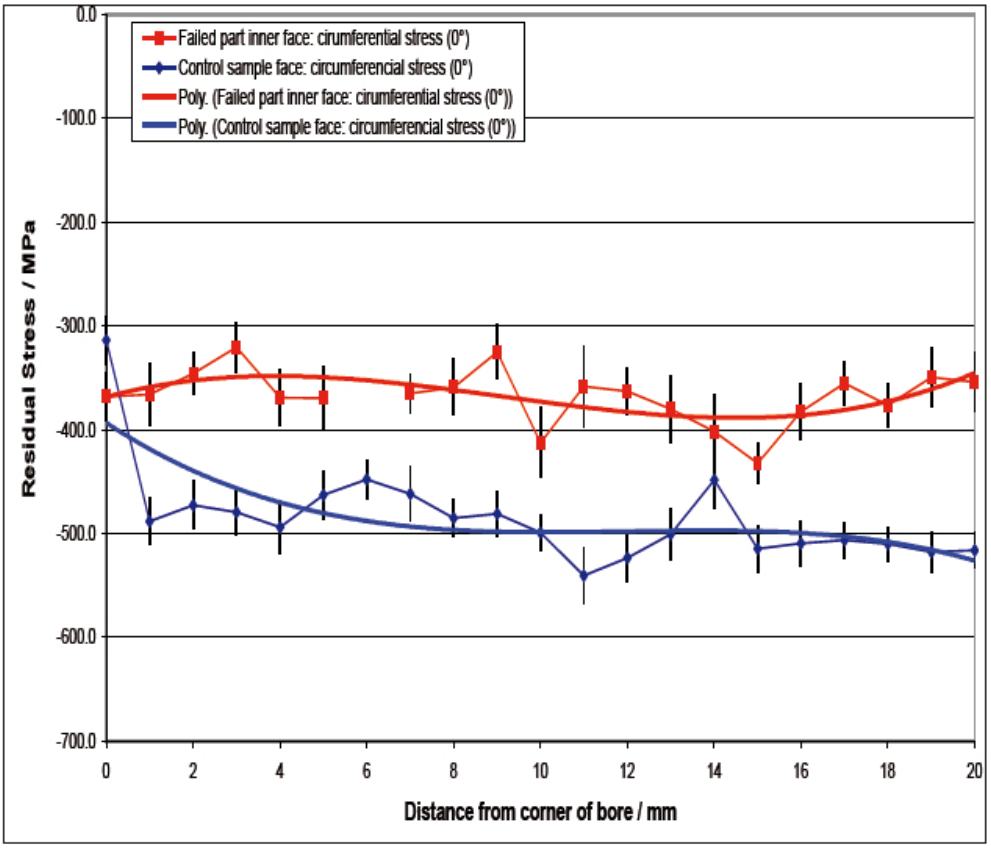

Figure 21

Plot of measured hoop stress at the inner face surface vs distance from corner of the bore

Manufacturer's measurements

The manufacturer initially carried out a series of residual stress measurements in the failed lug at two sites, one in the central region of the bore and the other in the central region of the inner face. Between each measurement, the surface locally at each site was progressively cut back over the very small measurement region so as to expose progressively the sub-surface material, and the stress measured at the newly exposed surface *at depth* measured and plotted to produce a stress gradient through the surface layer[3]. The results, which are reproduced at Figure 22, implied a residual compressive layer of some 600 MPa magnitude to a depth of approximately 100 microns, thereafter reducing to insignificant values at a depth of some 300 microns below the surface.

3 The diameter of the recess and the method whereby it was produced was chosen so as to minimise the probability of the stresses at the newly exposed surfaces being relieved by the processes employed or the changes of geometry produced.

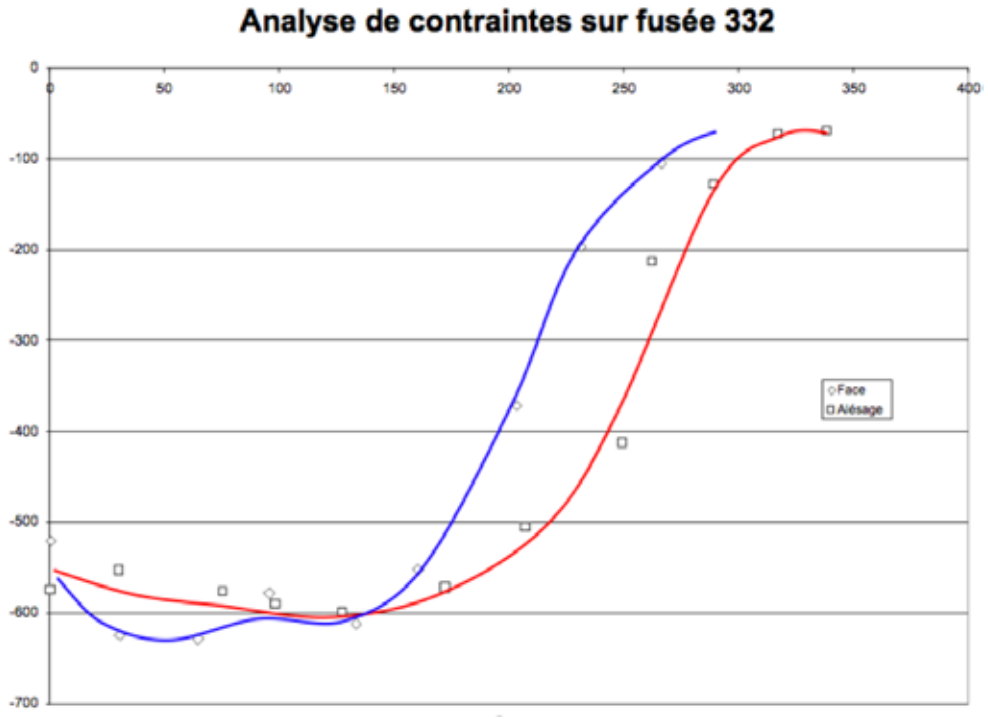

Figure 22

Plot of residual stress vs depth from surface for the failed lug, measured at locations near the centre of the bore (red) and inner face (blue)

Measurements of circumferential (hoop) and transverse residual stress were also made on a small region of the inner corner chamfer, at a position approximately midway around the corner profile. The two sets of measurements that were made indicated a mean compressive residual stress at the surface of 480 MPa circumferentially, and 500 MPa transversely.

Core properties

The general microstructures of the failed and intact yokes were very similar, and the hardness values obtained from the core region of the exemplar yoke and the failed yoke matched to within 1%.

1.12.4.4 Energy dispersive analysis (EDX)

Energy dispersive analyses (EDX) were carried out on the transverse section and the crack initiation region of the failed yoke, and also on the sacrificial washer.

Yoke

The yoke material comprised a low chromium steel, containing nickel, consistent with the specified material. Significant levels of cadmium were found in the bore of the yoke, both on the fracture surface generally and on the surface of a small recess at the crack initiation site. The former was assessed as corrosion product, emanating from the cadmium plating in the bore of the yoke. The cadmium found at the initiation site did not appear to be a result of post-fracture damage, and the recess itself was a pre-existing feature.

The exposed inner surface of the yoke that was originally covered by the sacrificial washer exhibited a considerable amount of corrosion product involving sodium, chlorine and sulphur, together with remnants of adhesive. Tungsten was also present, almost certainly originating from the tungsten-carbide wear-facing of the washer.

The particles of grit-like material found previously embedded in the yoke surface, beneath the adhesive used to attach the washer to the yoke, was shown to be aluminium oxide consistent with the products used in a grit blasting process.

The outer surface of the yoke exhibited a relatively uniform layer of cadmium.

The core section of the washer was found to comprise a low chromium steel containing nickel, similar to that of the yoke, and the wear-surface layer contained iron, cobalt, and tungsten, consistent with the sintered tungsten carbide coating specified.

1.12.5 Examination of the fractured inner washer

The inner sacrificial washer had fractured radially along a path substantially parallel with the yoke fracture, but displaced some 5-11 mm from it. The washer was also fractured along a path on substantially the same chord line on the opposing arm of the lug. Significant quantities of corrosion/fretting debris were present at and around both fracture sites.

Both washer fractures comprised a brittle *static* fracture through the carbide surface layer, followed by a fatigue fracture through the thickness of the underlying core material. The fracture on the lower half of the washer, next to the yoke failure, originated from the edge of the washer adjoining the flapping hinge and displayed extensive post-fracture corrosion.

1.12.6 Condition of the bore and bushing

The external surface of the bush installed in the failed lug exhibited localised regions of smearing and parallel scoring, aligned with the bore axis, consistent with the marks having been produced by an interference fit between the bush and the yoke at the time the bush was installed. Elsewhere on the outer surface of the bush, the original cadmium finish was largely unaffected.

The corresponding surface in the bore of the lug exhibited a similar pattern of localised surface damage to that shown by the bush, comprising smearing of surface high-spots in a direction parallel with the bore axis.

Remnants of the adhesive bond between the bush and the bore were also found adhering to the surfaces in several areas. Figures 23a and 23b show these features on the surface of the bore and the bush respectively.

Figure 23a

Surface condition in bore of failed lug

Figure 23b

Surface condition of bush

1.12.7 Detailed examination of the rotor head assembly

The complete rotor head from G-PUMI, less the failed Blue blade spindle, was shipped to the manufacturer's facilities where it underwent a detailed strip examination, dimensional and conformance checks, and assessment of condition by the manufacturer's specialists, overseen by a technical specialist from the BEA acting on behalf of the AAIB. Nothing abnormal was found, and all component parts were judged to be serviceable.

The rotor head was subsequently re-assembled – substantially as found but with a serviceable spindle substituted for the fractured component – and, after being instrumented with a system of strain gauges, was installed in a flight test aircraft. It was then flown in a series of test flights to obtain in-flight load data.

1.13 Medical and pathological information

Not applicable.

1.14 Fire

There was no fire.

1.15 Survival aspects

There were no injuries.

1.16 Tests and research

1.16.1 Studies carried out by the manufacturer

In consultation with the AAIB, the aircraft manufacturer set in train a wide-ranging study into the design and build of the variant of main rotor spindle involved. This work comprised:

1) A range of laboratory studies, including examination and dimensional checking of the inner bearing race and the subsequent discovery of traces of grease, found in the area of the fillet radius on the tie bolt. This discovery was judged to be highly significant, given the issues raised by the wear measurements of the inner bearing race. (**Appendix B).**

2) Detailed analysis and computer modelling studies of both the variant of spindle fitted to G-PUMI and relevant precursor variants, to better understand the deformation patterns and associated stresses in the yoke portion of the spindle under a range of applied loads and variations in physical condition, including:

   The effect of differing fits and clearances in the installed assembly, due to in-service wear at the various interfaces of the flapping hinge bearing.

   The effect of variations in the clamping pre-load applied across the yoke by the flapping hinge tie bolt.

   The effect of variations in damper-induced forces due to age and temperature-related changes in the dynamic characteristics of the frequency adaptor (lead-lag damper). (**Appendix C**).

3) A program of fatigue testing aimed at reproducing the mode of failure that occurred on G-PUMI. (**Appendix D**).

4) A program of flight trials in which the main rotor head from G-PUMI was instrumented, installed on a test aircraft, and flown to obtain flight load data for the spindle across the flight envelope, with each of the two relevant types of damper installed on the head whilst in service on G-PUMI. The data obtained from these trials underpinned both the theoretical analyses and fatigue testing referred to in items 1 and 2 above. (**Appendix E**).

5) A critical review of the assumptions and calculations made originally during the design and certification of the AS 332, and a review of this work using the latest available flight load spectra and the results of the stress distribution studies.

6) Investigations, with the BEA providing independent oversight, into the manufacturing processes and procedures employed during manufacture of main rotor blade spindles – both by the aircraft manufacturer and by the manufacturer contracted to supply the aircraft manufacturer with the type of blade spindle in question.

7) Investigations into the dynamic characteristics of the variant of frequency adaptor installed on G-PUMI at the time of the accident, and of the precursor variant initially installed on G-PUMI. The study included variations in stiffness and hysteresis of the rubber compound that provided the damping medium, due to aging, due to temperature effects, and due to recency of operation, ie to the time interval since the damper was last worked.

8) A study into the effects of bearing friction and related factors.

The studies yielded a significant body of experience and data that provided invaluable insights into the loading mechanisms, stresses, and deformations affecting the spindle yoke.

For brevity, only those aspects of the study work having direct relevance to the failure on G-PUMI are outlined in this report.

1.16.2 Manufacturing process

The aircraft manufacturer, with oversight from the BEA, conducted a review of the spindle manufacturer's production methodology, with particular reference to the shot-peening and related processes. Conformity with the specifications and drawings was confirmed, and no anomalies of significance were identified. Specifically, the shearing deformation of the grain structure observed in the shot-peen layer noted on the failed lug from G-PUMI (paragraph 1.12.3.3) was confirmed as being typical.

1.17 Organisational and management information

In this accident, Eurocopter (a company within the EADS international aerospace consortium) was the manufacturer and design authority for the AS 332L helicopter, and hence the holder of the Type Certificate for this aircraft type. Eurocopter provided investigators to assist the AAIB investigation immediately following the accident and continued to provide extensive support during the protracted and complex technical analysis, in concert with, and as Technical Advisors to, investigators from the BEA, following the protocols of ICAO Annex 13 ('*Standards & Recommended Practices'*).

The European Aviation Safety Agency (EASA) is the airworthiness regulator for the AS 332L type as France is the State of Manufacture. When Eurocopter produces safety actions, in the form of Alert Service Bulletins and other material, EASA considers this as the airworthiness regulator and may issue an Airworthiness Directive (AD), which makes the action mandatory for all operators.

1.18 Additional information

1.18.1 Air traffic control

After the helicopter stopped, the tower controller continued to manage the existing traffic movements. He was not aware that the helicopter had experienced a serious problem until the commander called and said he was going to shut down. It was at this point that a ground incident was declared and the emergency services alerted.

The tower controller commented that it was not unusual for a helicopter to land again immediately after takeoff, usually as the result of a minor problem. Such a problem would normally be quickly resolved and the helicopter would then be re-cleared for departure; this was what he had assumed to be the case on this occasion.

1.18.2 Development of the main rotor blade spindle in the AS 332 Super Puma helicopter

A summary of the development history of this spindle is in Appendix A and a summary of previous fatigue failures in Appendix F.

1.18.3 Safety actions taken in the course of the investigation

On the day of the accident, the manufacturer was advised of the AAIB's preliminary findings (summarised in paragraph 1.3 of this report) and invited to send specialists both to witness the work and to advise and assist with disassembly. There followed a close collaboration between the AAIB and the manufacturer, which was maintained throughout the investigation.

The following safety actions were initiated by the manufacturer during the course of this investigation:

1) A Telex notification dated 16 October 2006, addressed to all operators of AS 332 and AS532 aircraft variants, alerting them that an unexplained spindle lug failure had occurred, and providing a brief summary and photograph of the failed yoke in place.

2) Eurocopter Emergency Alert Service Bulletins, issued on 20 October 2006, 17 November 2006, and again on 9 September 2008, detailing checks of main rotor spindles on both installed and non-installed rotor heads. The aircraft types and inspection requirements covered by these Bulletins were initially widely cast, but were refined and focussed more specifically in the subsequent revisions as knowledge of the underlying issues advanced.

3) EASA Emergency Airworthiness Directive N° AD 2006-0327-E, dated 23 October 2006 applicable to all SA 330 and AS 332 variants. The AD required:

> *'...Not later than within 10 flight hours and thereafter at intervals not exceeding 10 flight hours [or in the case of AS 332 aircraft fitted with spindles P/N 332A31-1390 or P/N 332A31-1398, not later than within 5 flight hours and thereafter at intervals not exceeding 5 flight hours] check that there is no crack in the material section of the spindle yokes.'*

4) EASA Emergency Airworthiness Directive N° EAD No.: 2006-0349-E, Date: 21 November 2006, superseding and cancelling AD 2006-0327-E. This EAD introduced variations in the requirements for inspection called up in the original AD that differentiated between spindles incorporating the folding hinge option and those without, and specifying how the inspections were to be carried out by reference to Eurocopter Alert Service Bulletin N° SA 330 ASB No. 05.93.

5) SIN (Safety Information Notice) N° 2078-S-62, EASB 05.00.67 R2 and SB 62.00.74 were issued by Eurocopter in July 2009, which introduced a 'wet' assembly procedure, with new nuts, for the main rotor blade spindles and effectively eliminated the repetitive inspection procedure. This was endorsed and made mandatory by the issue of Airworthiness Directives (ADs) by the EASA.

The steps in (5) completed the analysis and safety actions by Eurocopter following this event, eliminating the repetitive inspection procedure by introducing a revised assembly procedure for the main rotor blade spindles.

2. Analysis

2.1 General

2.1.1 Operation of the flight

Up to the time of takeoff the flight was routine, with the commander ground taxiing the helicopter and the co-pilot conducting radio communications. The commander then handed control to the co-pilot for the takeoff as briefed. During the takeoff sequence a severe vibration started and the commander made an instant decision to stop. The helicopter was already five seconds into the calculated seven-second period to the critical decision point and immediate action was required, so the commander took over control from the relatively inexperienced co-pilot and aborted the takeoff. He also notified ATC of the nature of the problem. The helicopter came to a safe stop and the commander, after contacting ATC again, began to follow their instructions to vacate the active runway area. However, because of continued severe vibration he became concerned about the safety of the helicopter and decided to shut down the engines. Once the rotors had stopped the passengers were disembarked.

After aborting the takeoff the commander may have considered that the problem was temporary and that he would be able to taxi the helicopter clear of the runway. As soon as he attempted to do so he realised that it would not be possible and made the decision to shut down. The subsequent examination of the helicopter showed this shutdown decision to have been a sound and prudent action.

The action of the commander in aborting the takeoff was timely in preventing the helicopter from committing to being airborne, having suffered a serious structural failure of the rotor head assembly.

2.1.2 ATC recognition of emergency

Although the commander had relayed the information that the helicopter had experienced a bang and vibration the controller thought that just a routine minor problem had occurred and he continued to give clearances to land to other aircraft. It was only when the commander advised that he was shutting down his engines that the controller realised there was a serious problem and declared a ground incident. Other traffic movements on the airfield were then suspended until the helicopter had been moved to a safe area. Airfield operations were affected for a period of ten minutes.

The actions of ATC clearly had no influence on the structural failure and were prompt and clear.

2. 2 Physical characteristics of the failure

The spindle failed in fatigue, from a crack that had propagated through the lower section of the lug on the 'leading' side of the yoke. The fatigue crack originated at the inner corner of the bore accommodating the flapping hinge pin, and propagated through some 90% of the viable cross-section before the remaining 10% failed in overload.

2.3 Cause of the fatigue failure

A fatigue fracture through the lug portion of the spindle yoke was not a mode of failure anticipated during the design and certification of either the SA 330 or the AS 332. A small number of prior failures had occurred in service at this location, but all had been attributed to heavy fretting damage on design variants that preceded the introduction of the sacrificial washers, the purpose of which was to protect the yoke, specifically to address this fretting problem.

Following the introduction of the protective washers to address the fretting problem, no subsequent failures of the lug had occurred. Thus, the manufacturer's focus, in relation to the prevention of potential fatigue failures in service, reverted to the failure modes that had been identified during the course of the original certification assessment and fatigue testing, ie cracking from the origin sites in the fillet radius at the junction of the fork and barrel sections, and from the threaded section of the barrel.

The failure on G-PUMI was the first failure involving the variant of spindle with the '20 mm thick' yoke, and indeed the first involving a spindle incorporating protective washers to guard against initiation caused by fretting damage. The preceding lug failures had been perceived by the manufacturer as having being caused by a *localised* problem, addressed satisfactorily by implementation of the protective washers with no detailed underlying analysis of the failure mode. Consequently, there was no accumulated body of knowledge relating to the previous lug failures upon which the investigation could draw, and no failure mechanism was apparent capable of producing fatigue-damaging stresses in the lug.

It was necessary, therefore, to revert to first principles and to evaluate the factors that could have caused, or contributed to, the failure on G-PUMI. These ranged from the physical condition and material properties of the spindle through the processes employed in its manufacture, its operating and loading environments, its modes of flexure and the associated load paths. There was also the potential variability between spindle assemblies due to wear and tolerance stacking, as well as other variables affecting both the spindle components and the associated components in the main rotor head, such as the blade dampers.

2.3.1 Condition of the forging

No evidence was found of any significant surface defect in the origin region and the overall dimensions of the yoke and its material properties were within specification. The fillet radius at the origin was somewhat 'flattened', and was likely to have produced a marginally higher stress concentration locally than would have occurred if the profile had been precisely as specified. This factor alone could not explain the fatigue failure, but it could have been a second-order contributory factor.

Detailed investigation into the depth and intensity profile of the residual compressive stresses in the shot-peened surface layer (in the bore, on the face of the failed yoke and around the corner radius at the failure origin) showed a stress gradient that was broadly in line with expectations. Comparative studies of the residual stress profile from the failed G-PUMI forging and an exemplar forging suggested that the shot-peening on G-PUMI may have been slightly less effective than on the exemplar, producing residual compressive stresses in the area of interest that were possibly some 10% lower. However, without a much larger comparative study it was not possible to establish whether the shot-peening on the G-PUMI forging was significant. Overall, the evidence on shot-peening suggests that it may, at most, have been a second-order contributory factor.

In summary, no feature was identified in the failed forging that would have made it significantly more susceptible to fatigue than the other spindles in service. It follows, therefore, that the fatigue failure on G-PUMI must have been caused primarily by abnormally high working stresses in the area of the failure, with possible deficiencies in the corner radius geometry and the shot-peen layer making a contribution of second-order importance.

2.3.2 Flight loads

Nothing was found in the IHUMS record to suggest that any abnormal trend or condition occurred during the recorded period and post-accident flight testing, using the main rotor head components from G-PUMI except the failed spindle, confirmed that the load spectra used as the basis for certification fatigue testing, and the fatigue tests themselves, were valid.

The flight test data showed that the forces imposed by the lead-lag dampers (frequency adaptors) were by far the most significant dynamic load variable (as distinct from the quasi-static centrifugal loading) influencing the yoke stresses at the fracture origin site. It was also shown that the dynamic stiffness of the dampers, and hence the magnitude of the imposed forces they imposed on the spindle, were subject to variability that was a function of both age and recency of operation; the damper stiffness increases with time since manufacture and also with the time elapsed since the damper was last exercised. However, data from flights conducted with both of the damper sets installed on G-PUMI since the spindle in question was installed, following overhaul, showed that neither set would have induced fatigue-damaging stresses at the failure location.

In summary, the accumulated flight test data indicated that the failure was not likely to have been caused by abnormally high stresses resulting from in-flight loading, nor by abnormally stiff lead-lag dampers.

2.3.3 Built-in stresses in the spindle assembly

2.3.3.1 Potential stress-inducing mechanisms

Given that no abnormality of significance was found in the spindle forging, or in either of the damper sets installed on G-PUMI, nor in the spectrum of flight loads likely to have been encountered, it follows that the operating stresses at the failure origin must have been raised by some form of existing pre-load. In this regard, the finding of grease residues on the tie bolt is highly significant, particularly so given the wear identified on the end-faces of the inner race of the flapping hinge bearing. The combination of a wear gap and a potential means whereby the arms of the yoke could be flexed inwards, so as to close or partially close this gap, offers a mechanism that could lift the operating stresses at the critical section of the yoke to fatigue-damaging levels.

The relationship between the standing stresses induced in the yoke and the clamping force applied across it (the tie bolt tension) will depend primarily on whether there is a ‘tight’ or ‘loose’ fit between the flapping hinge pin and the

yoke/bush and, if a 'tight' fit, the degree of interference present. These factors will govern the modes of flexure adopted by the yoke as the clamping force closes the wear gap, and hence the distribution and magnitude of the associated stresses induced in the yoke.

Flexural modes with 'loose' fit at pin/bush/yoke interface

Figures 24a to 24c illustrate the modes of flexure that would occur in response to a progressively increasing tie bolt force with a 'loose' fit between the flapping hinge pin and the yoke.

Initially, from stage 1 to stage 2 (Figures 24a to 24b respectively), the yoke will flex freely inwards to close the wear gap. Until such time as it first comes into contact with the end face of the inner race (Figure 24b), its outer end will rotate bodily with the inner portion of the yoke arm, and no bending stresses will be induced in this outer region.

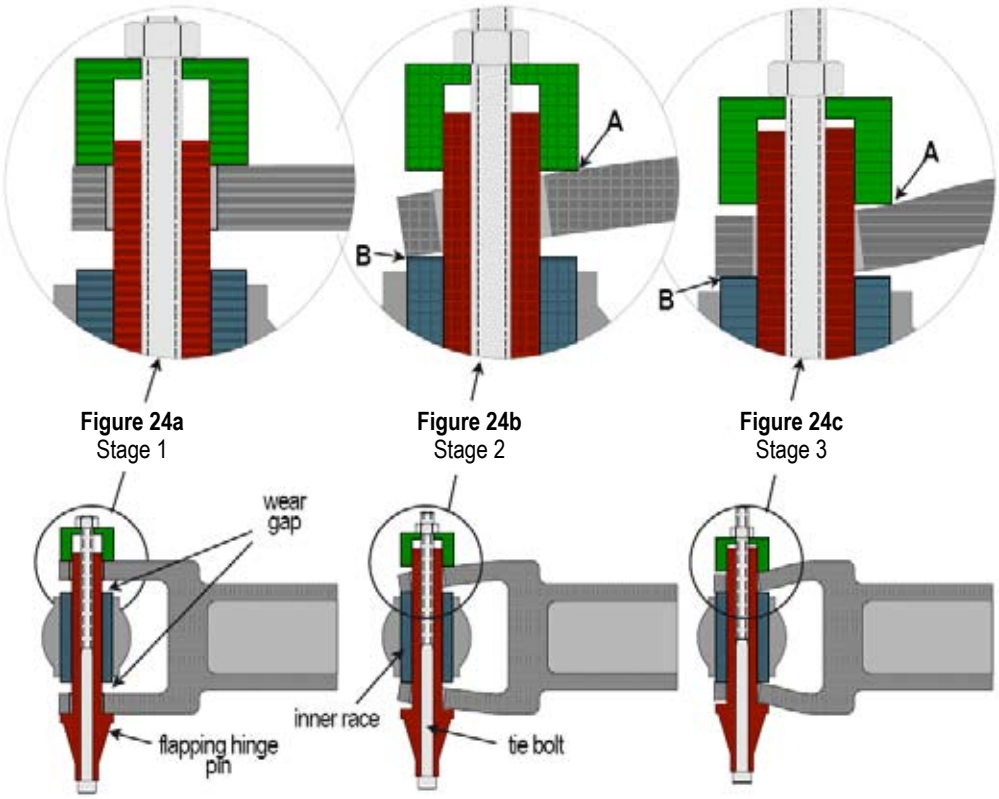

Figures 24a to 24c

Loose fit between hinge pin and yoke,
with no angular restraint between yoke and pin

Thereafter (stage 2 onwards), the reaction force imposed by the inner race will produce a reflex bend in the outer section of the yoke between the two contact points (A and B), generating an increasing tensile stress on the inner face of the yoke in the failure region.

This trend will continue as the yoke closes but, as the reflex bend increases, so will the clamping force be transmitted increasingly directly through the thickness of the yoke and into the inner race. The rate of stress increase during this latter stage will therefore reduce correspondingly.

Taken overall, the relationship between induced tensile stress (at the failure location) and pre-load (tie bolt force) would be expected to follow the general form shown in Figure 25. In this scenario, tensile stresses are produced solely as a result of the reflex bend profile, and arise only at relatively high clamping forces.

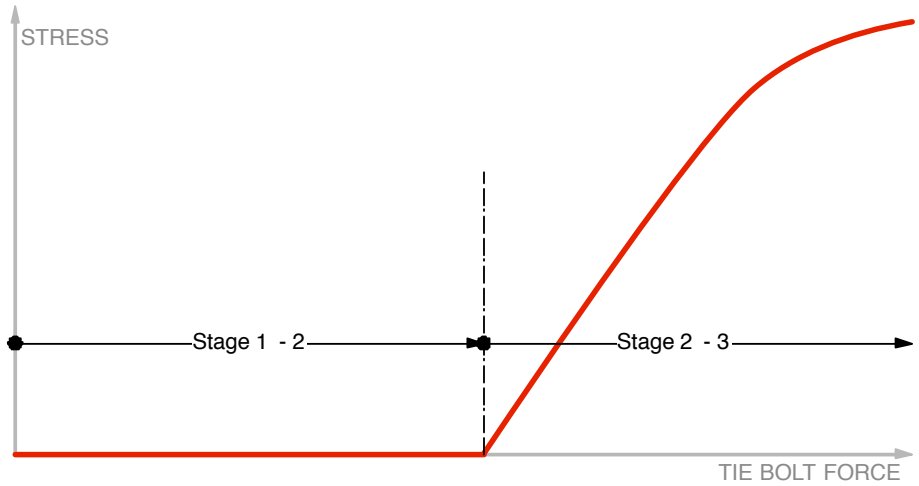

Figure 25

Expected trend of tensile stress vs applied clamping force

Flexural modes with interference fit at pin/bush/yoke interface

If there is a 'tight', or interference, fit between the flapping hinge pin and the yoke (Figures 26 a to c) then the outer end of the yoke will be forced to remain normal to the axis of the pin as the yoke arm deflects inwards. The bending reaction imposed by the pin on the outer end of the yoke arm will thus act directly to stretch the bore, inducing tensile stresses across it, and the outer part of the yoke arm will be forced into a reflex bend from the outset. A tensile stress will thus be induced across the bore on the inner face of the yoke increasing linearly with yoke deflection, as soon as the yoke starts to deflect in response to the applied pre-load.

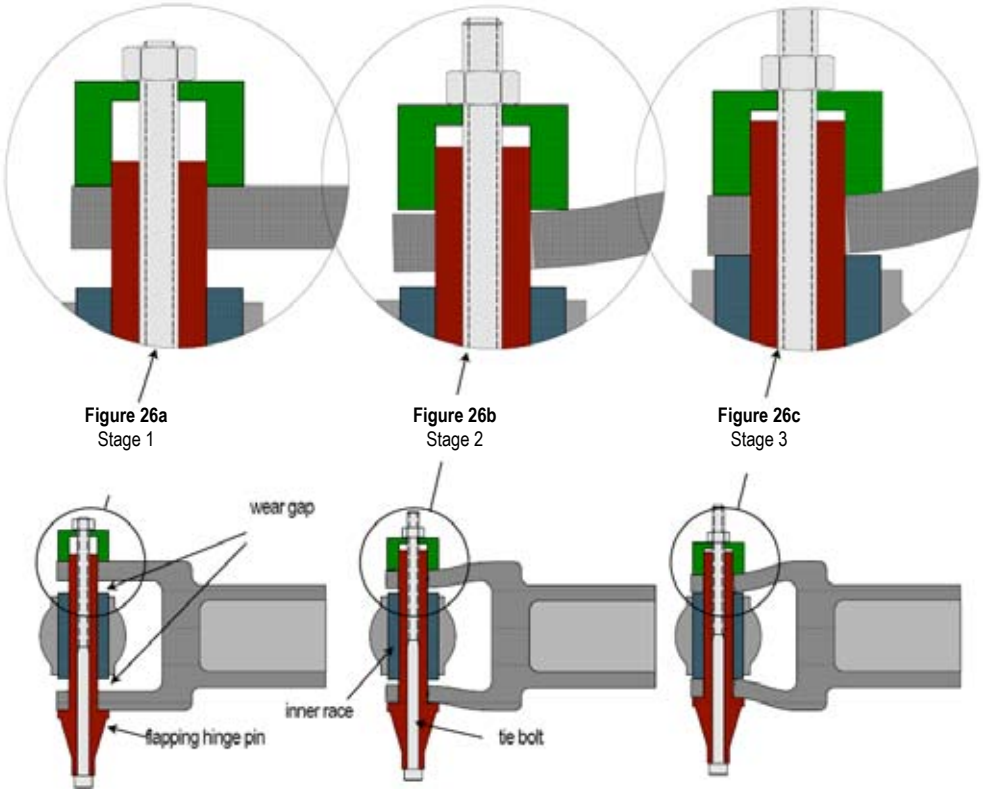

Figures 26a to 26c

Schematic showing effect of close or interference fit between hinge pin and yoke/bush, with angular restraint between yoke and pin

In this case therefore, the application of a pre-load will generate potentially much higher stresses across the inner face of the yoke, at the fatigue origin region, compared with those produced under similar loading conditions without there being a close or interference fit between the pin and the yoke. Tensile stresses due to an interference fit inducing strain across the bore of the yoke will be additive to these stresses.

Figure 27 shows the expected relationship between induced tensile stress (in the failure origin region) and tie bolt force. The lower curve is applicable to the case of a close-fitting pin without significant interference, and the upper curve is the case of a pin which has a significant interference fit.

In both cases, the tensile stress will increase as a substantially linearly function of pre-load bolt tension until the inner face of the yoke contacts the face of the inner race. Thereafter, further increases in tie bolt tension will increasingly be reacted directly through the stiffer path provided by the lug in contact with the inner race, with a correspondingly reduced rate of yoke flexure and associated

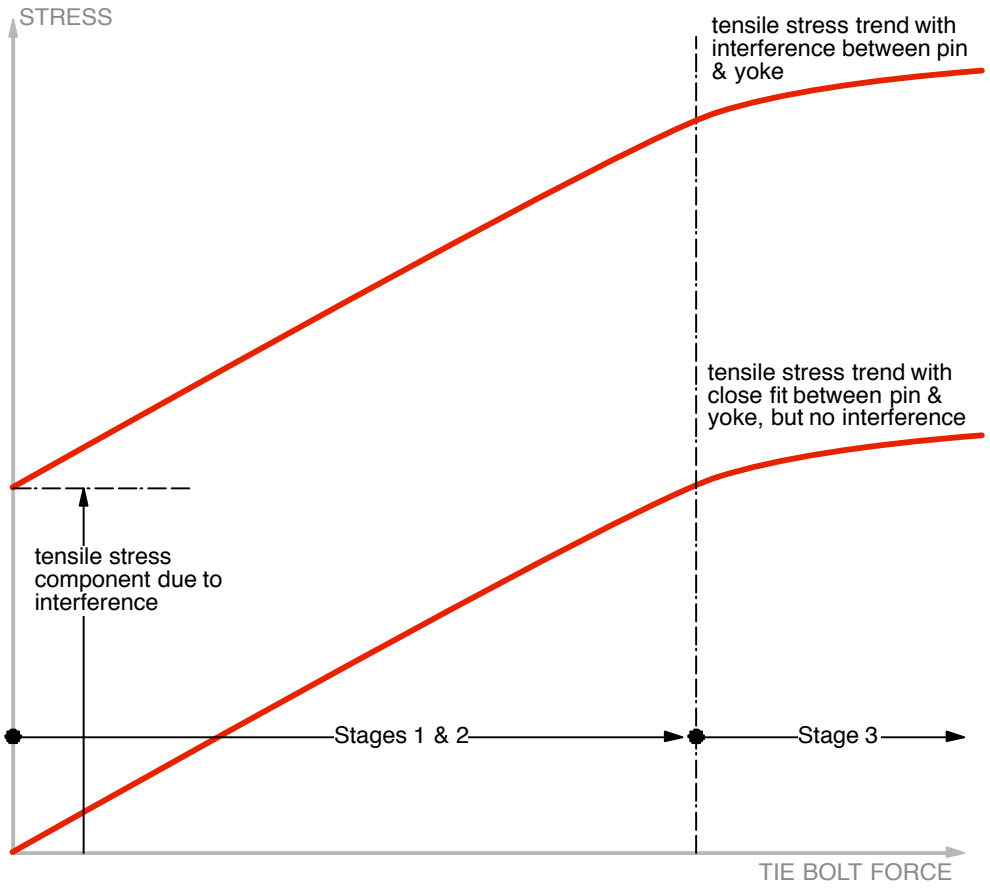

Figure 27

Expected trend of tensile stress vs applied clamping force
- tight or interference fit if pin/bush/yoke

tensile stress at the failure location. Interference between the hinge pin and the yoke/bush would tend to 'lift' the 'stress vs applied load' curve up the vertical ('stress') axis, by a value corresponding to the tensile stress induced by the interference strain across the diameter.

It is evident that the combination of a wear gap and a relatively tight-fitting pin would provide conditions whereby excessive tie bolt tension could generate potentially damaging stresses in the fatigue origin region, especially if combined with an interference fit. The generalised form of plots proposed in Figure 27 correlates well with the experimental results of the manufacturer's laboratory tests carried out to explore these effects, as shown in Figure 28.

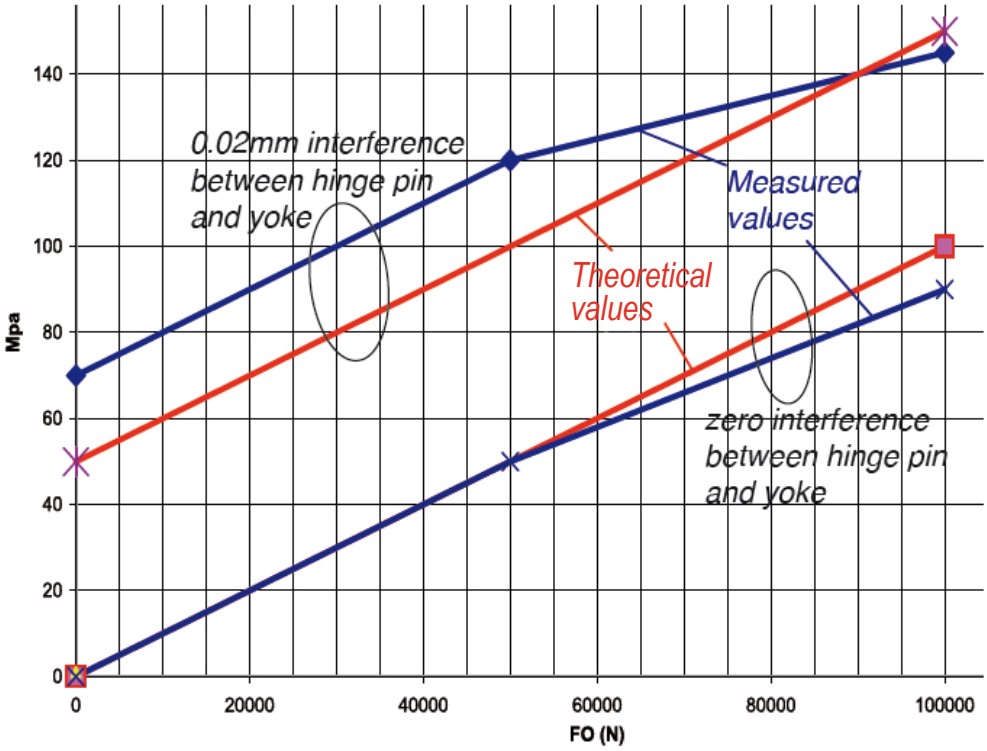

Figure 28

Stress on inner face of yoke at failure location as function of tie bolt preload

In relation to this scenario, each of the key factors potentially contributing to heightened tensile stresses at the fatigue initiation site appears to have been present on the failed spindle from G-PUMI:

Wear of 0.13 mm on the faces of the bearing inner race, close to the maximum wear exhibited within a sample of seven spindles studied.

Indications of grease on the tie bolt, tending to cause high tensile loads to be developed in the tie bolt when tightened to the specified torque value.

Scoring and associated features on the bush (paragraph 1.12.2 and Figure 23b) indicative of a significant interference fit at the time the components were installed. The interference present at the time the chilled bush was pressed into the yoke, producing the scores shown previously in Figure 23b, would have been increased further as the temperature of the bush rose to that of the yoke.

It is clear that the ingredients for the mechanism set out above were all present on G-PUMI, and that this mechanism was likely to have generated abnormally high operating stresses at the fatigue origin site, with second-order enhancements of this stress from the stress concentration at the corner radius and, possibly, reduced compressive (shot-peen) stresses in the surface layer at the corner. The question remaining, therefore, is whether these stresses could have reached levels sufficient to have initiated the fatigue fracture.

2.3.3.2 Theoretical analysis of potential flight loads

To assess the potential for the mechanism detailed in paragraph 2.3.3.1 to have caused the failure, a theoretical analysis was carried out by the manufacturer to estimate the maximum operating stresses that could have been generated in flight with this mechanism present. This analysis suggested that if the conditions listed below were present, a fatigue failure comparable to that on G-PUMI could be generated:

i) If the damper loads corresponded to the 'high-speed level flight' case (+/- 24,000 N), representative of offshore operations.

ii) If, due to grease on the tie bolt, a pre-load force of 100,000 N was present (as suggested by the laboratory tests in Appendix B) together with a wear gap sufficient to permit the yoke to flex in response to it.

iii) If interference slightly greater than that used in the laboratory tests were present at the pin/bush/yoke, such that the standing tensile stress induced at the fatigue origin site (in response to ii) would be increased from the140 MPa measured in the tests to 190 MPa.

Specifically, the analysis suggested that the conditions set out in i) to iii) above would result in a 10^{-3} to 10^{-4} probability of lug failure.

2.3.3.3 Application of yoke failure scenario to spindle variants with 15 mm yokes

An analysis by the manufacturer suggested that the application of the conditions listed in paragraph 2.3.3.2 items i) to iii) could explain the single, previously unexplained, case of lug failure affecting this variant of spindle.

2.3.3.4 Application of yoke failure scenario to sacrificial washer cracks

The approximate co-location of the yoke and washer fractures suggested that some common loading action had played a causal role in both the yoke and washer fractures.

The washer fractures each comprised a brittle static fracture of the carbide layer, followed by propagation of a fatigue fracture through the backing material from origin sites in the root of this static fracture. Neither the static nor the fatigue fractures were of significance in the overall failure, but the location and orientation of the washer cracks (parallel with, but slightly inboard of, the yoke fracture) is fully consistent with the yoke failure causal mechanism proposed in paragraph 2.3.3.1. Specifically, the deflection of the yoke arms, and hence of the washers bonded to them, as the tie bolt is tightened would put the carbide layer into tension – producing the static fracture – and the washer's location on the outside of the bend would have induced a standing tensile stress in the washer, contributing to the subsequent fatigue propagation through the backing material.

It is considered highly significant that, under these conditions, the position of maximum bending deformation of the washer, the expected line of fracture, will be slightly inboard of the hinge pin axis at approximately the positions identified in the schematic diagram Figure 29 (a reproduction of Figure 26c, amended to include the inner pair of washers).

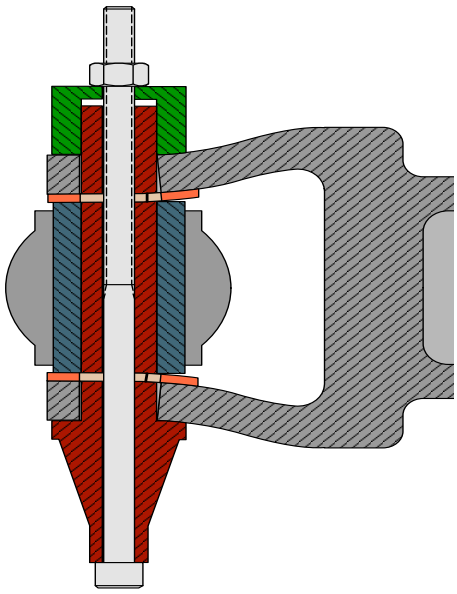

Figure 29

Schematic showing coincidence of maximum bending stress and location of the washer cracks

2.4 Failure period

2.4.1 Propagation period

The pattern of irregularly spaced beach marks evident on the fracture face, interspersed with large numbers of much finer striations, is consistent with the repetitive crack growth pattern that would be produced by the step change in centrifugal loading between each rotor stop and subsequent start. The intervening finer striations are consistent with the higher frequency alternating flight loads imposed on the blades between each stop-start cycle. The number of beach marks discernible on that part of the fracture, from when it first broke through to the visible surface of the yoke, corresponded to some 15 -17 rotor starts, which, from aircraft's flight history, involved some 47-54 flight hours (and 126-133 landings).

The beach marks produced during the preceding stages of growth, extending from the origin up to the point when the crack first breached the visible surface, were less clearly defined and a precise analysis of this part of the fracture could not be made. The best estimate that could be made, which involved extrapolation of markings across the less clearly defined regions of the fracture, suggested that this period involved some 73 rotor stop-start cycles, equating to some 210 flight hours. Overall, therefore, the evidence suggested that the crack propagated from origin to final failure over a period involving some 90 rotor starts, and 258 flight hours.

2.4.2 Initiation period

It was not possible to determine with accuracy the crack initiation period, as distinct from its propagation period. Under laboratory test conditions, with test specimens having a good (fine) surface finish, an initiation period an order of magnitude higher than the propagation to failure period would not be unusual. In real world conditions, however, with components having a less perfect surface finish, a shorter propagation period would be expected.

In this case, interpretation of the fracture produced during the post-incident fatigue testing suggested a ratio of 'initiation time to propagation time' of approximately 11:1. However the test set-up was designed to provide reliable crack initiation, rather than reliable propagation, data.

Therefore, at the request of the AAIB, the manufacturer conducted an analysis of the variable propagation conditions. This suggested that, under realistic conditions, the ratio of 'initiation to propagation' of the crack on G-PUMI

was of the order of 0.5, a propagation period twice the initiation period. Based on the total propagation period of about 258 hrs, inferred from the fracture faces from G-PUMI, this ratio would suggest an initiation period of about 129 hours, making a total period to failure of about 387 hrs.

2.4.3 Initiating event

Whilst uncertainty must attach to the estimated total period of approximately 387 hrs to failure, this figure does suggest that the primary causal factors were not likely to have been present from the time of overhaul (1,558 hours before failure). However, a detailed trawl of the maintenance records showed that the tie bolt was removed only once in the period following the overhaul, in September 2006 when all four frequency adaptors were replaced, 175 hours prior to final failure.

Given the level of uncertainty in the estimated period of 387 hrs, and that the later tie bolt removal and re-installation (171 hours before failure) represent the sole disturbance since the spindle's installation following overhaul, it is likely that the critical combination of wear gaps and excessive tie bolt tension came into being at this time. This is almost certainly due to the bolt coming inadvertently into contact with extraneous grease on the flapping spindle as it was inserted prior to the nut being torqued to the specified value.

2.4.4 Safety actions and Recommendation

Following the discovery of the yoke fracture in G-PUMI, safety measures were taken expeditiously by the manufacturer and endorsed by the airworthiness regulator, the EASA. These measures were principally frequent visual inspections of the affected components and are detailed in paragraph 1.18.3. These frequent inspections remained in place as development work by the manufacturer led to changes to hardware and to the assembly process for the main rotor head. These changes in assembly and hardware, introduced by Eurocopter in July 2009, eliminated the repetitive inspection procedure by introducing a revised assembly procedure for the main rotor spindle, endorsed and mandated by the EASA in Airworthiness Directives (ADs).

At an early stage in the investigation the AAIB and the CAA discussed the possibilities and limitations of current HUMS technology for detecting defects of the kind that occurred in G-PUMI. The CAA has continued to be active in the development of HUMS technology and the potential exists for sensors in the rotating portions of helicopter dynamic systems, to assist in

early detection of defects. As the EASA has responsibility for Continued Airworthiness of this category of aircraft, therefore:

It is recommended that the European Aviation Safety Agency, with the assistance of the Civil Aviation Authority, conduct a review of options for extending the scope of HUMS detection into the rotating systems of helicopters.
Safety Recommendation 2010-027

3. Conclusions

a) Findings

The accident flight

1) The flight crew were properly licensed and qualified to conduct the flight.

2) The flight crew were suitably rested and held valid medical certificates.

3) Five seconds after lifting off to begin a flight to the Britannia Platform, the lower half of the lug forming the leading side of the Blue main blade spindle yoke fractured.

4) The failure was accompanied by a bang and very heavy vibration, and the crew immediately landed back on Runway 14. The aircraft was shut down and the passengers disembarked whilst still on the runway.

The fracture mechanism

5) The yoke had failed in fatigue, due to a crack that originated at the corner radius on the inner end of the bore in the lug that accommodates the flapping hinge pin. The fatigue crack propagated through some 90% of the cross-section before the remaining material became overloaded and ruptured.

6) Analysis of the fracture faces indicated that the primary fatigue crack had propagated over a period of some 90 rotor starts, with the crack breaking through the visibly accessible lower surface of the lug 15 to 17 rotor starts prior to the final rupture.

7) The aircraft's flight logs indicated corresponding flight times of 258 hrs for propagation to failure, of which 47-54 flight hours occurred after the crack had broken through the visible lower surface of the yoke.

8) Sacrificial washers bonded to the inner faces of the lugs were also cracked along fracture lines parallel with the plane of the yoke fracture.

9) Flight loads measured in flight trials were broadly comparable to those upon which the original design and certification, including fatigue testing of the spindle, was based. The minor differences were inconsequential in any potential primary causal mechanism.

10) None of the fatigue testing had identified any potential failure of the yoke section of the spindle and failures had involved the main body of the spindle.

11) Failures of the spindle lugs had occurred in service at positions comparable to the G-PUMI failure, only on earlier designs of spindle with thinner (15 mm) yokes.

12) Initiation of earlier fractures had been attributed to fretting between the inner face of the yoke and the flapping hinge inner race with no sacrificial washer, to be introduced later specifically to prevent fretting failures of this type.

13) No significant deviations from specification or drawings were found in the failed blade spindle forging, or any of the associated components.

14) Evidence of wear was found on the end faces of the flapping hinge bearing inner race, the extent of which was close to the maximum measured across a small sample of spindles undergoing overhaul by the aircraft manufacturer.

15) Traces of grease were found on the tie bolt passing through the centre of the flapping hinge pin and laboratory testing showed that application of the specified dry torque to a lubricated tie bolt induced a pre-load substantially higher than the manufacturer intended.

16) Excessive tie bolt tension, due to grease, combined with wear gaps between the yoke inner faces and the ends of the hinge bearing inner race, will cause the yoke arms to deform inwards and adopt a reflex mode of flexure which induces significant standing (static) stresses in the yoke at the fatigue origin site.

17) It is likely that only trace amounts of grease had contaminated the tie bolt, introduced unwittingly as the tie bolt came into contact with extraneous grease in the bore of the flapping hinge pin, as the bolt was reinstalled. In such circumstances, there would have been no indication to the person installing the bolt that contamination had occurred.

18) The superposition of alternating stresses, caused by in-flight loading, onto these large standing stresses was shown to create conditions capable of fatigue crack initiation at the fracture site.

(b) Causal factors

The investigation identified the following causal factors for the failure of the spindle yoke:

(i) Wear on the flapping hinge inner race.

(ii) Excessive clamping pre-load across the yoke, due to the tie bolt being torqued to the specified dry value in the presence of grease when the tie bolts were reinstalled some 175 hours prior to failure of the yoke.

(iii) Significant hoop stresses in the bore of the yoke due to adverse tolerance stacking and the associated interference fit of the bush in the yoke.

(c) Contributory factors

The investigation identified the following factors which may have contributed to the failure of the spindle yoke:

(i) Flight loads biased towards the high speed level flight condition, slightly higher than those generated by normal level flight cruise conditions.

(ii) A minor deviation in corner radius profile at the inner end of the bore, with a small increase in the attendant stress concentration.

(iii) A minor reduction in the intensity of the compressive surface layer stresses from the shot-peen process, at the fatigue origin site.

(iv) Flight loads in the spindle yoke slightly higher than anticipated in certification fatigue testing, due to the action of the lead-lag dampers (frequency adaptors).

(Fatigue testing carried out by the manufacturer in support of the investigation replicated the failure on G-PUMI precisely, under test conditions which incorporated the Causal factors above, together with Contributory factor (i), above. The mode, location and orientation of the failure of the washers on G-PUMI are fully consistent with these factors).

4.0 Safety Recommendation

Safety Recommendation 2010-027: It is recommended that the European Aviation Safety Agency, with the assistance of the Civil Aviation Authority, conduct a review of options for extending the scope of HUMS detection into the rotating systems of helicopters.

.

Mr Robert Carter
Inspector of Air Accidents
Air Accidents Investigation Branch
Department for Transport

Appendix A

Development of main rotor blade spindle in AS 332 Super Puma helicopter

Design change milestones

The SA 330 Puma and AS 332 Super Puma blade spindles share a common genesis in terms of both their original design, and the changes and improvements introduced subsequently were informed by service experience gained on both types.

The original AS 332 Super Puma spindle design, part number 330A31.1122.09, was based on the original SA 330 Puma design with 15 mm thick lugs in which the bores were shot-peened. The shot peening induced a residual compressive stress in the surface layer, which was intended to reduce susceptibility to fatigue initiation in response to the hoop stresses developed in the yoke in reacting the combination of quasi-static centrifugal blade forces and dynamic flight loads.

Unlike the original Puma spindles, the AS 332 variant incorporated a protective bushing in the bore of the lug, bonded in place and then line bored in situ. However, like its progenitor, the sole protection on the faces of the lug - at the interfaces with the flapping spindle and its associated bearing faces - comprised a coat of Graphoil varnish overlaying the cadmium-plated and painted finish applied to the yoke overall. Figure 30 is a sectional view through the yoke of the original AS 332 spindle, showing the protective bush, the extent and position of the shot-peened surfaces and surface coatings applied.

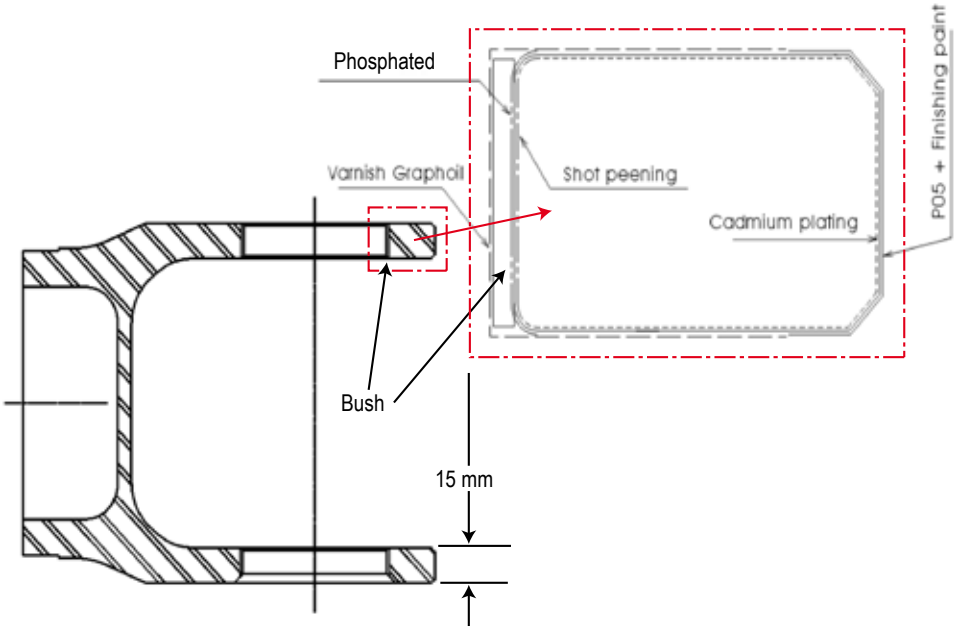

Figure 30

Section through original design variant

Appendix A

In light of the two lug failures experienced in service in 1981, and of the fatigue failure that occurred, in 1982 in particular, which was attributed solely to fretting initiation at the interfaces between the lug and the flapping hinge spindle and associated bearing parts, the design of the yoke was revised to incorporate:

Sacrificial anti-fretting washers, faced with tungsten carbide, bonded to the faces of the lug.

Shot peening of the lug faces, in addition to the existing peening of the bores, to improve resistance to fatigue initiation.

There followed a number of minor revisions to the design, including changes to the barrel portion of the spindle of no direct relevance to this investigation before a new design was introduced, see Figure 31, with the following changes:

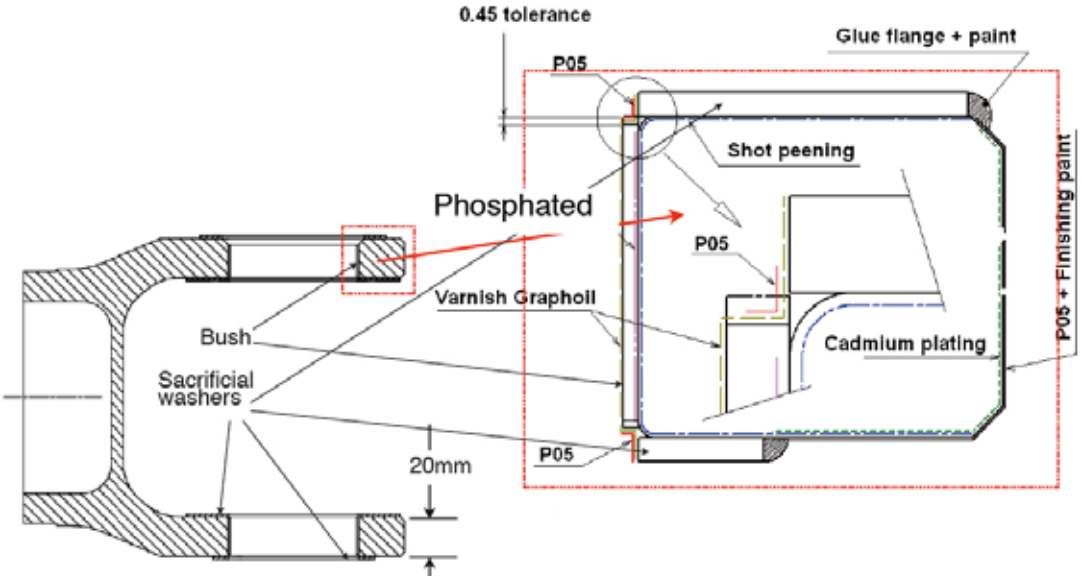

Figure 31

New design spindle part N° 332A31.1410.02, (thicker lugs + sacrificial washers)

An increase in lug thickness from 15 mm to 20 mm.

Sacrificial washers bonded to both inner and outer faces of the lugs.

A revised flapping hinge pin, incorporating a single-rose-jointed lead-lag damper attachment spigot, and a tie bolt through which a clamping pre-load was applied across the yoke.

Appendix A

More extensive shot-peening of the lug surfaces.

Additional protective treatments applied to the lug surfaces.

Figure 32 is a sectional view through the revised yoke and flapping spindle assembly, showing:

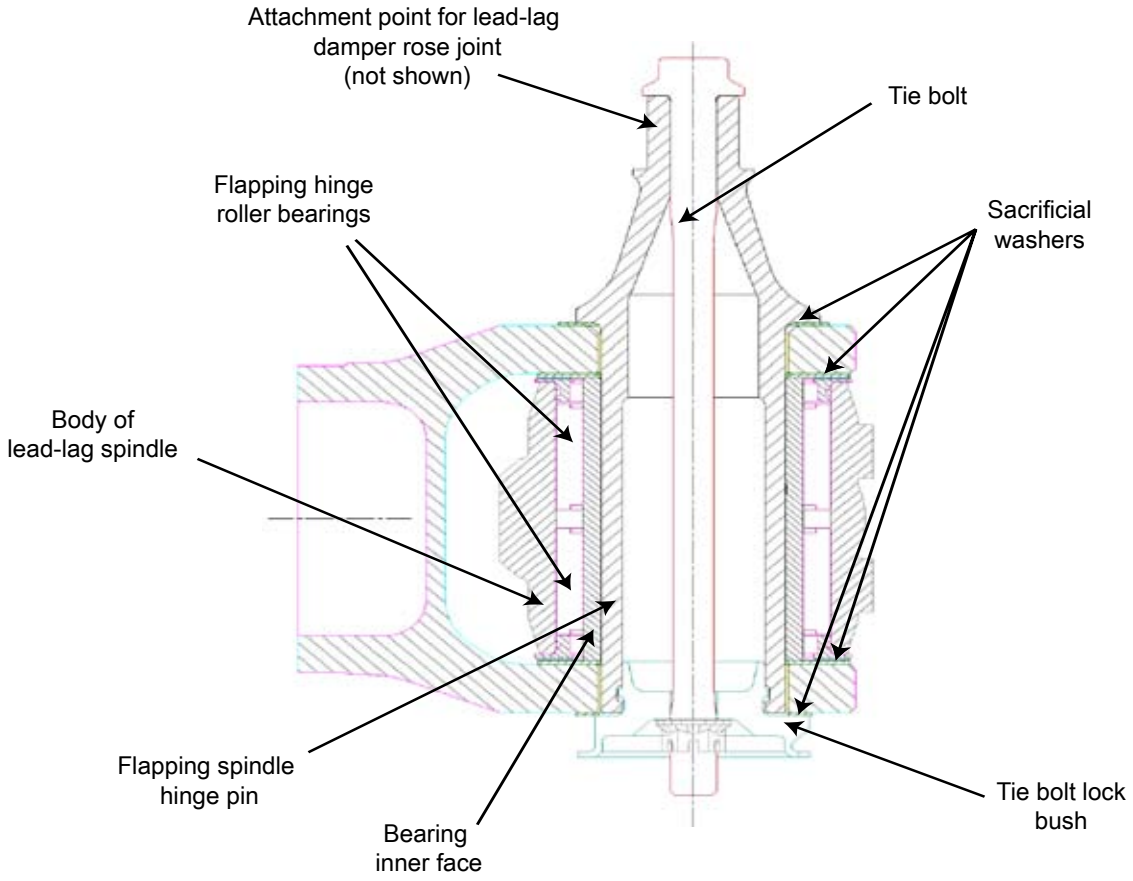

Figure 32

New design yoke & flapping spindle assembly – sectional view

The flapping spindle roller bearing.

The new design flapping spindle, with offset spigot to accommodate the rose-joint damper attachment bearing.

The tie bolt running through the centre of the spindle.

The sacrificial washers. (See Figure 2b for installation details)

Appendix A

A full listing of changes made to the Super Puma blade spindle, with relevant part numbers, is given in the table below.

PART N°	DETAILS	TYPE APPLICABILITY
330A31.1122.09 & 10	Original design for the AS 332 MK1, based on the 'SA 330 Puma' 15mm thick lugs on yoke portion.	AS 332 SUPER PUMA + SA 330 PUMA
332A31.1390.02	New design in light of 1982 fatigue failure, incorporating anti-fretting washers	AS 332 SUPER PUMA + SA 330 PUMA
332A31.1390.03	Post Mod 07.43.088: new anti-fretting washer with tungsten carbide deposit	AS 332 SUPER PUMA + SA 330 PUMA
332A31.1390.05	Post Mod 07.43.113: Graphoil D 148 deposit on the spindle barrel	AS 332 SUPER PUMA + SA 330 PUMA
332A31.1390.06	Post Mod 07.43.131: increased flapping hinge angle	AS 332 SUPER PUMA + SA 330 PUMA
332A31.1390.07	Post Mod 07.43.165: Addition of a bush inside the spindle barrel to improve the resistance of the threads	AS 332 SUPER PUMA + SA 330 PUMA
332A31.1390.08/09 & /10	New fabrication with increased thickness of the barrel under the threads (…/09 or /10 suffix, depending of the origin of the casting)	AS 332 SUPER PUMA + SA 330 PUMA
332A31.1398.00 or 332A31.1398.05/06/07	Post Mod 07.43.233 (relocated seal): 332A31.1398.00 (retrofit spindle P/N 332A31.1390.07) or 332A31.1398.05/06/07 (retrofit spindle P/N 332A31.1390.08/09/10)	AS 332 SUPER PUMA + SA 330 PUMA
332A31.1410.02	New spindle design, post-mod 07.43.100 (yoke lug thickness increased from 15mm to 20mm + new flapping hinge pin incorporating tie bolt) and post-mod 07.43.143 (increased thread Service Life Limit)	AS 332 SUPER PUMA only
332A31.1410.03	Post-mod 07.43.167: Addition of bush inside spindle barrel to improve the resistance of the threads	AS 332 SUPER PUMA only
332A31.1410.04 or .05	New fabrication with increased thickness of barrel behind threads. (.04 or .05 suffix, depending on casting manufacturer)	AS 332 SUPER PUMA only
332A31.1485.00, or 332A31.1485.05 or .06	Post Mod 07.43.233: repositioned seal, becomes 332A31.1485.00 (retrofit of spindle 332A31.1490.03) or 332A31.1485.05 or 06 (retrofit of spindle P/N 332A31.1485.04 and 05).	AS 332 SUPER PUMA only

Appendix A

Certification

The spindle was subject to fatigue testing for certification purposes in 1987. During those tests a pattern of repeated loads was applied representative of the centrifugal loads, damper loads, and blade pitch-change loads based on data from instrumented flight trials that provided rotor system load spectra across a range of flight conditions. The tests took into account the increase in stiffness of the lead-lag dampers with decreasing temperature, down to a minimum of -50°C which mapped to a 44% increase in the dynamic in-plane bending moments imposed on the blade spindle.

A total of eight blade spindles were tested, during the course of which fatigue cracks were produced that propagated through the main barrel of the spindle from two origin regions: one was sited in the radius at the junction between the yoke and the barrel portions of the spindle and the other in the fillet radius at the threaded section, see Figure 33.

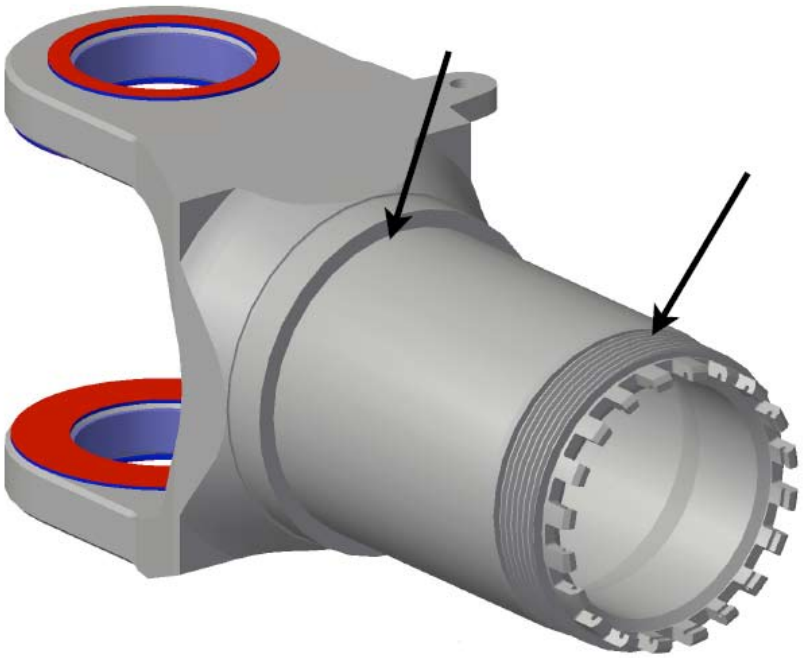

Figure 33

Location of the origins of fatigue cracks produced during the certification fatigue test program

The fatigue tests also induced fatigue cracks through the thickness of the anti-fretting washers bonded to the faces of the yoke, from fretting origins on surfaces interfacing with the flapping spindle. These washers were designed as sacrificial components, to protect the lug from fretting-induced fatigue cracking, and, because no cracks were induced in the

lug at any stage during testing, it was deemed that the washers were fulfilling their function satisfactorily.

Prior to the investigation of the spindle failure on G-PUMI, none of the manufacturer's fatigue susceptibility analyses had suggested any condition or loading action that would predispose the lug sections of the yoke to fatigue failure.

Appendix B

Study by the manufacturer - Laboratory studies

A range of laboratory studies was carried by the manufacturer during the course of this investigation. Much of this work, although necessary and worthwhile, in the event did not contribute materially to understanding the failure on G-PUMI. Those which did contribute are summarised below:-

Condition of the inner bearing race

Measurements of the overall length of the flapping hinge inner bearing extracted from the failed blade spindle on G-PUMI implied a total loss of material from the two end-faces of the race of 0.12 mm, ie some 0.12 mm of wear in total.

Measurements of spindles from the fleet passing through the manufacturer's overhaul facility revealed the corresponding total wear. This data implied that the extent of wear on the component from G-PUMI was broadly typical of what might reasonably be expected of in-service components, albeit close to the more extreme end of the spectrum.

The apparent prevalence of wear at the yoke/inner race interface raised questions as to the potential effect wear at this location could have on the stresses at the failure origin region, due to yoke deformation, should the tie bolt exert a clamping force capable of closing this gap. In particular, it offered a potential means whereby the yoke arms could adopt a reflex bending profile that would not otherwise occur, with an attendant induced tensile stress at the failure site.

Presence of grease on the tie bolt

Traces of grease were found in the area of the fillet radius on the tie bolt. This finding was judged to be potentially of great significance, given the issues raised by the wear measurements detailed in the preceding paragraph. Specifically:

1) Grease on the tie bolt could increase substantially the tension induced in the tie-bolt when its nut was tightened to the specified torque loading during assembly, potentially sufficient to close the any wear gap present and,

2) Cause the yoke arms to adopt a reverse (reflex) bend that could potentially induce signficantly high the tensile stresses in the yoke at the failure location.

Appendix B

*Measured stress with a wear gap **and** excessive tie bolt tension*

These studies were prompted by the trace evidence found of grease on the tie bolt from G-PUMI, and the realisation that a combination of excessive tie bolt tension (which would result if dry torque values were applied to a lubricated bolt) **and** a wear gap could potentially increase the standing stresses in the yoke at the failure location.

A series of bench tests was devised to determine the stresses developed in the lugs of the yoke as functions of:

1) Variation in the size of wear gap between the inner faces of the yoke and the end faces of the bearing inner race, over the range 0.046 mm to 0.16 mm.

2) Variation in the magnitude of the clamping force over the range zero to 100,000 N, the effect of the pre-load applied by the tie bolt, tending to deform the yoke and close the wear gap.

3) Variations in the interference fit between the flapping hinge pin and the yoke, over the range 0.01 mm to 0.02 mm.

Figure 28 shows the recorded stress at the inner face of the yoke at the failure location, as a function of tie bolt tension (pre-load). The measured values are coloured dark blue. The red plots are the theoretical values, based on a relationship derived from the FE analysis but corrected to account for the standing stress induced by the diametral interference between the flapping hinge pin and the yoke. Taking due account of the limited range of conditions tested, and extrapolating from the ~145 MPa maximum stress recorded during the tests, the manufacturer concluded that with grease on the tie bolt, standing stresses as high as 190 MPa could potentially be developed during assembly of a spindle with both wear and grease present.

Appendix C

Study by the manufacturer - Finite element analysis (FEA)

FEA studies

A preliminary FEA carried out by the aircraft manufacturer provided a range of coarse preliminary data, but the model lacked the sophistication required for detailed study. A specialist company was therefore contracted to undertake a more refined analysis using SAMCEF FEA code, which offered an enhanced capability for simulating the combined effects of:

1) Clearances at various sites within the yoke assembly, to simulate the effects of gaps at various key interfaces,

2) Clamping pre-load across the yoke, the tension in the tie bolt.

A separate FEA was undertaken in which the stresses in the sacrificial washers alone were studied.

Scope and objectives - yoke assembly

The principal FE model, (Figure 34), was optimised to explore the deformations and associated stresses in the yoke generally, and the stresses in the vicinity of the failure origin on G-PUMI specifically, as functions of the following parameters:

1) Pre-load only, the effect of tie bolt tension alone, with no external load applied.

2) Pre-load + centrifugal blade loading.

3) Pre-load + centrifugal blade loading + lead-lag bending moment + positive and negative lead-lag shear loading.

4) Flapping hinge stiffness.

5) Shear load induced by the pitch-change horn; included for completeness because this aspect had not been included in any of the fatigue tests carried out previously.

6) Blade moments simulating abnormal bearing wear.

Appendix C

7) The effect of *wear gaps* at the various mechanical interfaces between the yoke and the flapping hinge components.

The pre-load was based on a tie bolt tension of 50,500 Newtons (N)

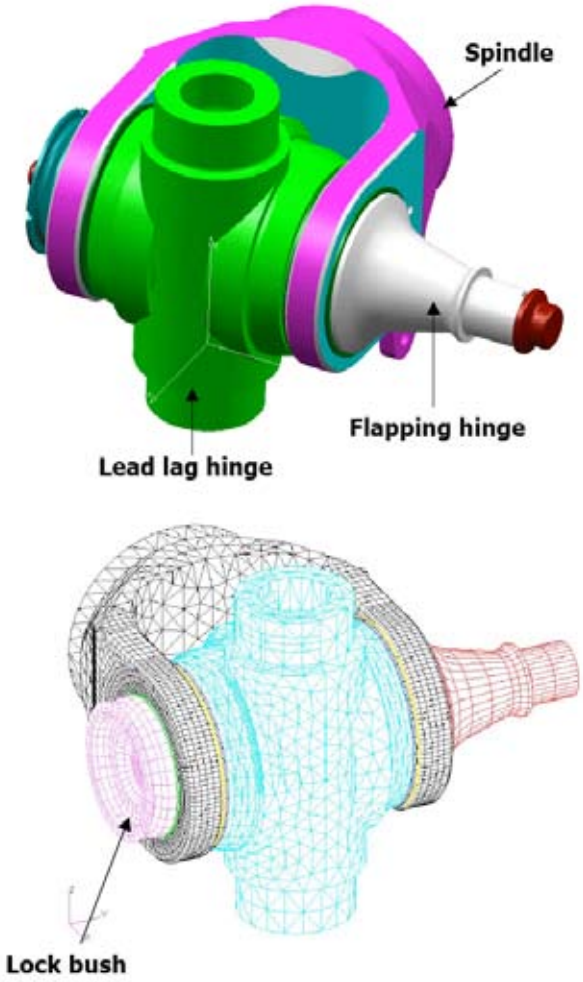

Figure 34

FE model detail

It was not possible to model accurately the stiffness profile across the adhesive layer attaching the sacrificial washers to the yoke, but this aspect was the subject of a separate appraisal at a later stage, on the strength of which it was judged as being of secondary influence and of no practical significance to the results obtained.

Appendix C

FE model results - yoke assembly

The results of the FEA studies suggested that, within the range of parameter values studied, and with the tie bolt pre-load set to 50,500 N:

1) Neither variations in the vertical shear force (the 'lift' component of the centrifugal load imposed by the blade) nor the horizontal shear force (associated with the damper-imposed restrain on lead-lag movement of the blade) had any significant effect on the stress in the failure origin region.

2) Variations in the force applied through the pitch-change horn had no significant effect.

3) Neither a '*bad*' pitch change bearing nor a '*bad*' lead-lag bearing had any significant effect on the lug stress at the failure location.

4) Centrifugal blade force + blade-drag shear force, with zero damper-induced bending moment, produced the asymmetric pattern of deformation of the yoke shown (in much exaggerated form) in Figure 35a.

5) The addition of damper-induced lead-lag bending forces increased both the extent of flexure and the asymmetry, see Figure 35b.

6) A stress concentration was identified under most loading conditions that coincided with location of the failure origin on G-PUMI, at the inner corner of the bore of the lug on the leading side of the yoke, see Figure 36.

7) The magnitude of this stress at the failure origin exhibited a substantially linear correlation with variations in each of the key loading parameters, of which the damper load was by far the most dominant factor. However, within the range of feasible flight loads, the magnitude of this remained substantially below the threshold at which fatigue crack initiation would be expected.

8) It was not possible to model the corner radius in the failure origin region with a sufficiently small mesh size to predict with confidence the stress concentration factor due to the radius geometry per se, but a simplified analysis of this geometry was undertaken using a chamfer of comparable dimensions, which is a more critical case. The results indicated that a stress concentration of the order of 1.2 was likely to apply at the corner radius, the local stress at the radius was likely to be some 20% above the baseline values predicted by the model.

Appendix C

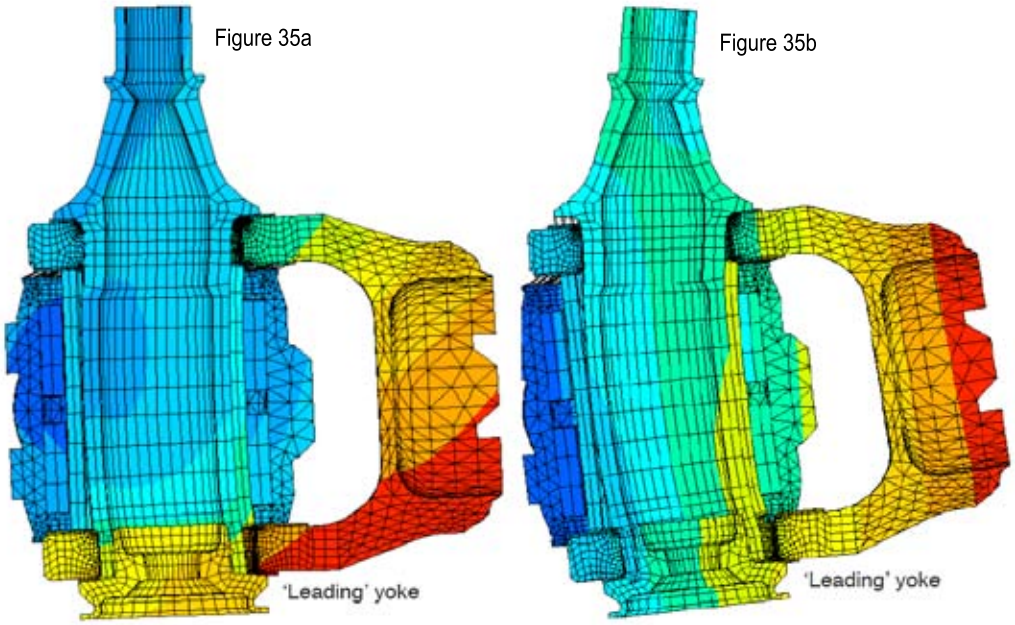

Figure 35a

Deformation pattern with centrifugal and blade-drag shear loading only

Figure 35b

Deformation pattern with centrifugal + lead lag bending moment applied through damper attachment on flapping spindle extension

The model results suggested that variations in the gap between the yoke and the flapping hinge bearing inner race would not have influenced significantly the stress at the failure origin region, but intuitively this finding was considered questionable validity – suggesting that the FE model was deficient in modelling this aspect. The combined effects of wear gaps and excessive tie bolt tension (as distinct from the deficient tension explored in the flight tests) were therefore the subject of a separate laboratory study, described in Appendix B, in which representative static loads were applied to an instrumented spindle incorporating both these aforementioned features.

Appendix C

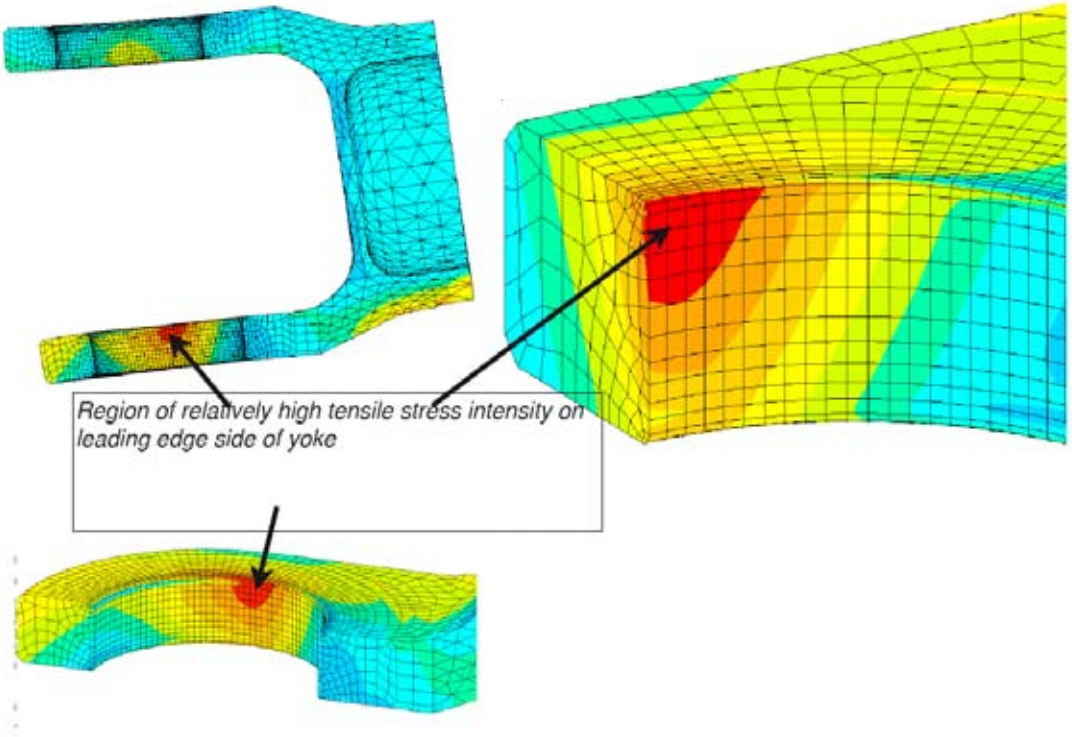

Figure 36

Position of maximum tensile stress at the surface adjoining the inner corner
in the bore of the lug on the leading side of the yoke,
at approximately the failure location on G-PUMI

FE model results - sacrificial washer only

The FEM results predicted a maximum stress for the level flight case that was almost identical to the value determined previously during work underpinning the certification of the revised design of spindle incorporating these washers.

Appendix D

Study by the manufacturer - Fatigue tests

Tests on failed spindle from G-PUMI

Test setup

A series of fatigue tests was undertaken over several phases using both sample blade spindles from the fleet and the failed spindle from G-PUMI.

The blade spindle to be tested was clamped securely to an anchored fixture and subjected to a schedule of repeated loads applied through one lug of the yoke only. The approach allowed the surviving half of the failed yoke from G-PUMI to be tested. The loads were applied through a forked clevis, connected to the (single) lug of the yoke by a clevis that replicated the flapping hinge pin. The use of a clevis ensured that a balanced load was applied to the lug under test, that no bending couple was introduced between the line of action of the applied load and the lug axis. The application of load to one half of the spindle yoke only introduced an unavoidable offset between applied and the overall reacting force, and consequently a non-representative couple was applied to the overall system. However, the rigidity of the yoke barrel and shoulder regions, when mounted in the fixture, was such that this couple could be reacted without the arms of the yoke flexing to a degree that would influence signficantly the stress field developed in the *working* half of the yoke under test. For all practical purposes, therefore, the fatigue tests were adjudged to replicate adequately the conditions that would have existed if the loading action had been applied symmetrically to both halves of the yoke.

The loaded yoke lug was instrumented with a series of eight strain gauges, four on each side of the lug at the critical (mid) location of the lug failure on G-PUMI, and the outputs from these were recorded and monitored during all fatigue testing.

Phase 1 testing

The initial phase of testing was carried out using a sample spindle from the fleet, and a loading schedule comprising a repeat alternating pattern of high-cycle/low-amplitude, and low cycle/high amplitude, applied loads. Each high cycle/low amplitude segment comprised a series of 0.1×10^6 reversals about a mean stress of 380 MPa at the critical location, with stress reversal amplitudes starting at +/- 63 MPa for the first segment, and increasing in stages through each of nine subsequent segments to a maximum of +/- 193 MPa. Between each of these segments, an intervening segment of low cycle fatigue was applied each comprising a sequence of 10 load applications inducing solely tensile stresses at the failure location of rising from a baseline value of 32 MPa to 485 MPa and back to 32 MPa.

Appendix D

After completion of a total of 10 of these patterns of high cycle/low cycle loading segments, broadly comparable to the program of fatigue testing undertaken during the original certification of the revised spindle design in 1985, the spindle remained intact with no discernible signs of cracking.

Phase 2 testing

During the phase 2 testing, the phase 1 pattern of loading was repeated using the failed spindle from G-PUMI as the test subject. This resulted in a fatigue failure through the body of the spindle after 0.37 x 10^6 reversals, from a fatigue crack originating in the fillet radius at the junction between the barrel section and the yoke, see Figure 37.

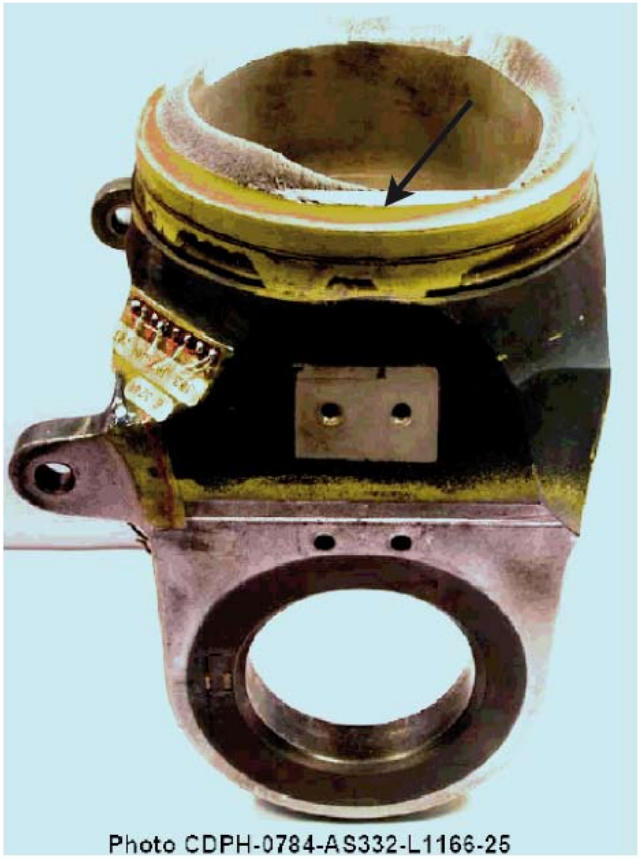

Figure 37

Fatigue test failure of G-PUMI spindle,
from origin at radius of the barrel section (arrowed)

This mode of failure was substantially similar to failures produced during previous fatigue testing for certification of the revised spindle design.

Appendix D

Phase 3 testing

The sample spindle used for the phase 1 tests was reinstalled in the test rig and the overall sequence of loading used for the phase 1 tests was repeated, but this time with the applied loads increased so as to raise the mean value of the high cycle stresses to 560 MPa at the *yoke failure* location. This value reflected the potential for excessive standing stresses in the yoke to be induced during during assembly, based on the laboratory investigations into the effects of grease on the tie bolt, wear gaps, and the interference fit of the flapping hinge pin in the yoke. The magnitude of the alternating stress superimposed on this mean for the phase 3 test was also increased from that of the previous tests, to 217 MPa.

After completion of 0.5 x 10^6 reversals, no failure had occurred and the magnitude of the alternating stress component was increased from 217 to 245 MPa.

After completion of a further 0.375 x 10^6 reversal at this increased magnitude, a fatigue fracture occurred through the lug at the location of the G-PUMI failure, see Figure 38. However, the origin of this failure was in the bore of the lug, set back some 4.2 mm from the inner corner radius, whereas the G-PUMI fracture origin was actually coincident with the inner corner radius itself.

Figure 38

Fatigue test failure (arrowed) at location G-PUMI failure, but with origin 4.2 mm from corner radius

Appendix D

Phase 4 testing

For the phase 4 test, a second spindle from the fleet was installed in the rig and the phase 3 loading pattern was repeated but with the mean stress increased to 670 MPa at the critical (lug failure) location, and an alternating stress amplitude of +/- 206 MPa.

After 10^6 reversals, no failure had occurred and the magnitude of the alternating stress was increased from 206 to 258 MPa.

After a further 0.5503 x 10^6 reversals the yoke fractured in fatigue through the lug, at the failure location on G-PUMI, see Figure 39. The origin of this fracture was sited actually on the inner corner radius, replicating precisely for all practical purposes the failure on G-PUMI.

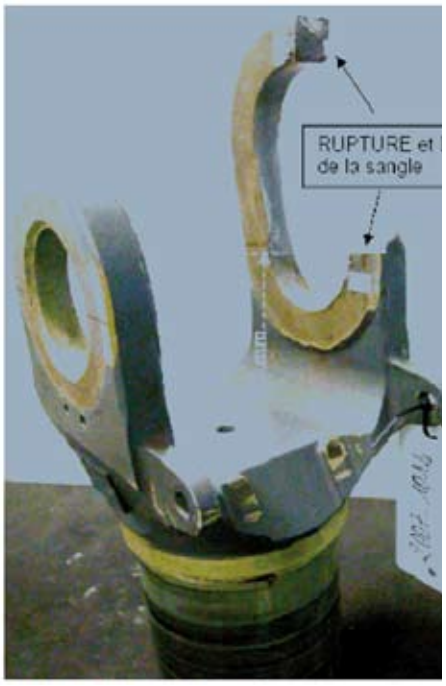

Figure 39

Fatigue test failure (arrowed) at location of G-PUMI failure,
with origin at inner corner radius

Laboratory examination of the fractures faces by the manufacturer suggested that the crack had propagated to failure over some 0.05 x 10^6 load cycles. Theoretical analysis of the damage accumulated during the initial 10^6 load cycles (at the lower level) without failure, during which the induced stress was very close to the estimated fatigue limit, suggested that it would have contributed some 3.7%, with the second phase (higher) loading sequence which produced the final failure contributing the remaining 96.3% of the damage. On that basis, it was estimated that the crack initiation period was of the order of 0.5 x 10^6 cycles.

Appendix E

Study by the manufacturer - Flight tests

Scope and objectives

A series of flight tests was carried out by the manufacturer utilising a representative airframe on which had been installed the complete rotor head assembly from G-PUMI. The aircraft weight and CG were comparable to those of the certification test flights carried out previously, before the introduction of the revised design of spindle incorporating the 20 mm thick yoke and sacrificial washers.

The head was rebuilt to its 'installed' state on G-PUMI except for the following differences:

1) Installation of new rotor blades at all positions.

2) Switching of the spindle installed originally at the Yellow blade position to the Blue blade position, and installation of the bearings and related components removed from the original (failed) blue spindle into this new blue (ie the originally yellow) spindle.

3) Installation of a new (unused) spindle at the yellow blade position.

4) Substitution, at different stages during the testing, of the two variants of lead-lag damper (frequency adaptor) fitted to G-PUMI over the period of interest, always fitted as type-matched pairs on opposing blades.

5) Installation of strain gauge instrumentation and associated data recording systems, optimised to measure the in-flight stresses on the spindle as close to the failure location in the yoke as practicable; and installation of strain gauges on associated components chosen to provide a detailed history of the-flight loads acting on spindle and related components.

The data obtained from the flight tests was analysed with the following objectives:

1) To establish, across all phases of flight, the stresses acting on the yoke at the failure location.

2) To characterise the stresses generated in the spindle due specifically to the constraints on blade motion imposed by the elastomeric lead-lag dampers (frequency adaptors).

3) To quantify the effects, in terms of the flight loads acting on the spindle, of changes in damper characteristics - both the *operating time* and *age-related* variations in stiffness and hysteresis of two variants of damper installed on G-PUMI during the relevant period.

4) To explore the effects on working stress at the failure location of a reduction in the torque applied to the flapping hinge tie-bolt. Specifically, the effect of a reduction in the clamping force applied across the yoke by the tie bolt, below that produced by the lower limit of the specified torque to be applied during assembly.

6) To compare the loads obtained from the flight trials with those from the original flight test programme, used as the basis of the *certification* fatigue test programme.

7) To establish whether variations in the condition of the flapping hinge bearings and related components (*used* versus *new*) could affect materially the working stress at the failure location.

Flight regimes

The flight regimes explored during the testing encompassed the following: Taxiing, Hover, Climb, Level flight at 130 kt, Levels flight V_{MAX}, Flight at V_{NE}, Banked turns to left and right (at speeds of 125 kt – 130kt and bank angles of 30°, 45°, and 50°), Autorotation, Descent, Normal approach.

Summary of flight test results

The pitch link loads measured on opposing sides of the head (Yellow and Blue) were similar to one another, and comparable to the values obtained and used for certification purposes previously.

It was established that once the centrifugal load had built to its working level, the stress at the failure location thereafter was governed primarily by the restraining forces imposed on the blade system by the lead-lag damper, via the extension of the flapping hinge spindle; they were not influenced significantly by variations the forces imposed by the pitch-change rods, nor by reductions in tie bolt tension, a reduction in the torque applied during installation of the tie bolt, below the specified figures.

Appendix E

The damper-induced stress at the failure location measured during flights with the *new* variant of damper (the variant installed on G-PUMI some 171 flight hours before the failure) was some 13% greater during turning manoeuvres to the left, and 20% higher during turns to the right, than the corresponding stress measured during flights with the worn '*old variant*' dampers installed previously. In level flight, the stress at the failure location was some 10% higher with the '*new*' dampers installed than with the '*old*' dampers. Ground-based measurements of the dynamic stiffness and hysteresis of the two sets of dampers suggested that the new ones were some 7% stiffer than their old counterparts. The greater dynamic stiffness of the newer units explained, in part at least, the higher stresses measured during the flights when these were fitted, certainly the 10% increase noted in level flight. The even larger increases observed during turning manoeuvres could not be fully explained, but it was felt that some variability was to be expected given the small size of the data set, and the potential for variations to occur in the precise manner in which individual turning manoeuvres were flown.

In level flight, the maximum stress measured at the failure location was some 37% higher than the corresponding maxima measured during the original flight trials of the '*new*' design of spindle (with the 20 mm thick yoke), carried out in 1986. During turns to the left, they were some 17% higher, and during turns to the right they were some 50% higher. Differences of up to 15% could be explained by the natural variation in dynamic stiffness between units which have been recently '*worked*' and those '*not worked*' for a period (unworked units tend to stiffen-up slightly over a period of non-use), but an unexplained discrepancy of around 20% remained.

Significant discrepancies were apparent between the stiffness values measured on the later variant of damper by the aircraft manufacturer, using its own ground-based equipment, and the values measured on the same units by the damper's manufacturer at the time they were originally produced. Further investigation suggested these differences were real; caused by post-production age-related stiffening.

A review of damper loads measured in level turns during the course of other flight trials carried out by the manufacturer in the intervening period between the original certification trials and the investigation flight trials identified a number of occasions when comparable flight loads were produced, and, after due consideration, the manufacturer concluded that the original certification flight data may have been questionable, rather than the more recently acquired data.

Appendix F

Summary of previous fatigue events (SA 330 Puma and AS 332 Super Puma)

The following events were identified as fatigue crack events in SA 330 Puma and AS 332 Super Puma helicopters, preceding the event in G-PUMI:

YEAR	A/C TYPE & CIRCUMSTANCES	SPINDLE HOURS	SPINDLE P/N	NOTES
1981	PUMA (SA 330) Detected during overhaul	1488	330A31 1122.03	15mm15mm thick Yoke. Fatigue crack in bore of leading edge yoke. Significant fretting evident. Crack propagation tests conducted by manufacturer.
1981	PUMA (SA 330) No details available	2624	330A31 1122.03	15mm thick Yoke. Fatigue crack in bore of leading edge yoke. Cause assessed as "bad" rework during overhaul. Overhaul procedures improved.
1982	SUPER PUMA (AS 332 Mk1) Just after take off from rig. Noise + severe vibration. Immediate landing	406	330A31.1122.09	15mm thick Yoke. Fatigue crack in bore of leading edge yoke. Manufacturer estimated crack propagation period ~39 hrs. SB 05.02 (82.32) (CN 82-131-3(B)) & later SB 01.01 (83.01) issued in response.
1986	PUMA (SA 330) Level flight. Noise + heavy vibration. Flight continued; landed safely 15 min later	1054	330 A31 1122.09	Fatigue crack in bore of leading edge yoke. Fretting origination at the yoke internal face.
1988	PUMA (SA 330) No details available	1183	330 A31 1122.09	Fatigue crack in bore of leading edge yoke. Fretting origination close to the radius at end of contact between bushes and yoke. One strap of yoke completely failed; secondary fatigue crack on remaining strap a (no failure).